JGR Atmospheres

RESEARCH ARTICLE
10.1029/2020JD033474

Fate of Pollution Emitted During the 2015 Indonesian Fire Season

Mijeong Park[1], Helen M. Worden[1], Douglas E. Kinnison[1], Benjamin Gaubert[1], Simone Tilmes[1], Louisa K. Emmons[1], Michelle L. Santee[2], Lucien Froidevaux[2], and Chris D. Boone[3]

[1]National Center for Atmospheric Research, Boulder, CO, USA, [2]Jet Propulsion Laboratory, California Institute of Technology, Pasadena, CA, USA, [3]Department of Chemistry, University of Waterloo, Waterloo, ON, Canada

Key Points:

- Anomalously high carbon monoxide (CO) emitted during the 2015 Indonesian fire season was transported into the upper troposphere and lower stratosphere
- Satellite measurements of hydrogen cyanide (HCN) indicate that wildfires can have an impact on the HCN concentrations in the stratosphere for up to 2 years
- Community Atmosphere Model with Chemistry simulations reproduce increases in CO in October 2015 but underestimate the amount of CO compared to the measurements

Correspondence to:
M. Park,
mijeong@ucar.edu

Citation:
Park, M., Worden, H. M., Kinnison, D. E., Gaubert, B., Tilmes, S., Emmons, L. K., et al. (2021). Fate of pollution emitted during the 2015 Indonesian fire season. *Journal of Geophysical Research: Atmospheres*, *126*, e2020JD033474. https://doi.org/10.1029/2020JD033474

Received 8 JUL 2020
Accepted 10 APR 2021

Abstract The El Niño-driven fire season in Indonesia in September–October 2015 produced the largest fire emissions on record since NASA's EOS satellites started making observations of tropospheric pollutants from space. In this study, measurements of carbon monoxide (CO) from the Measurement of Pollution in the Troposphere (MOPITT) on Terra and the Microwave Limb Sounder are used to characterize the anomalously high CO emitted during the 2015 Indonesian fire season transported into the tropical upper troposphere and stratosphere. The satellite measurements indicate that CO emitted from wildfires was transported into the upper troposphere with time lags up to ~2 months and continued to be transported into the stratosphere, which resulted in higher concentrations of CO extending up to ~20 hPa by the end of 2016. Hydrogen cyanide (HCN) measured by the Atmospheric Chemistry Experiment Fourier Transform Spectrometer (ACE-FTS) confirms that anomalously high HCN emitted from the same wildfires was also transported into the tropical stratosphere and persisted throughout 2017. Simulations of CO from the Community Atmosphere Model with Chemistry (CAM-chem) show a significant increase in CO concentrations in the troposphere in October 2015. However, comparisons between CAM-chem and MOPITT CO suggest that the model underestimates the amount of CO even with doubled emissions of CO in October 2015. Both the satellite measurements and the model simulations show that the pollution emitted from the wildfires over Indonesia was transported to and persisted in the tropical stratosphere much longer than the previous El-Niño driven fire events due to unprecedented amount of the fire emissions.

1. Introduction

Large-scale climate variability, such as El Niño conditions, can have a significant impact on the physical and dynamical processes in the atmosphere. In the tropics, changes in large-scale circulation and convection during El Niño events perturb atmospheric chemical composition (e.g., Duncan, Strahan, et al., 2007; Logan et al., 2008; Nassar et al., 2009). Severe drought conditions in the tropical western Pacific associated with El Niño can lead to intense wildfires in Indonesia (e.g., Page et al., 2002; Tansey et al., 2008; Field et al., 2016; Sheese et al., 2017; Pumphrey et al., 2018; Pan et al., 2018) that can have a direct impact on human health (Mead et al., 2018). These changes in surface emissions and large-scale circulation affect the distribution of long-lived tracers, such as carbon monoxide (CO), in the tropical upper troposphere and lower stratosphere. CO, one of the major pollutants emitted from wildfires, has a chemical lifetime of ~2 months (Duncan, Logan, et al., 2007; Holloway et al., 2000) in the tropical troposphere, and hence it is a suitable tracer to study atmospheric transport processes (e.g., Park et al., 2009; 2013; Huang et al., 2014).

Previous studies have shown perturbations in the distributions of CO, ozone (O_3) and water vapor (H_2O) in the upper troposphere and lower stratosphere (UTLS) during the 2006 El Niño event using both satellite measurements and a global chemistry model (Chandra et al., 2009; Logan et al., 2008; Nassar et al., 2009; Ott et al., 2010). The 2015 El Niño was one of the most severe on record over the past two decades (Santoso et al., 2017). Satellite measurements of CO in the troposphere (Field et al., 2016) and hydrogen cyanide (HCN) in the stratosphere (Pumphrey et al., 2018; Sheese et al., 2017) show significant atmospheric impact of surface emissions from wildfires in Indonesia during and after the fire season. Emissions produced by wildfires can influence both dynamics and chemistry in the UTLS. Chemically, CO contributes to O_3 production in the upper troposphere via NOx–HOx–CH_4–O_3 smog chemistry and by changing hydroxyl

radical (OH) concentrations, indirectly affecting HOx catalytic loss reactions (Bey et al., 2001; Kinnison et al., 2001). The CO lifetime in the upper stratosphere varies depending on the season and latitude (Minschwaner et al., 2010), ranging between 10 and ~30 days. In the lower stratosphere, CO has a longer lifetime of a few months and is a sink of OH (Rinsland et al., 2000). Therefore, a CO increase also affects trace gas lifetimes, including that of CO in the stratosphere (Duncan, Strahan, et al., 2007). Dynamically, pollution in particular of radiatively absorbing aerosols like black carbon can change atmospheric circulation by altering diabatic heating rates (Ott et al., 2010 and references therein).

The impact of the strong 2015 El Niño on tropospheric and lower stratospheric composition lasted for several months (Field et al., 2016; Mead et al., 2018; Nechita-Banda et al., 2018; Pumphrey et al., 2018). In this study, our goal is to characterize the anomalously high CO emitted during the 2015 Indonesian fire season transported into the tropical troposphere and stratosphere. Long-term satellite observations of CO covering the troposphere and stratosphere are used with a focus on the period up to 4 years after the 2015 fire season ended. The Measurement of Pollution in the Troposphere (MOPITT) on Terra provides CO vertical profiles in the troposphere (Deeter et al., 2019; Drummond et al., 2010), and retrievals from the Microwave Limb Sounder (MLS) on Aura cover the vertical range from the upper troposphere to the mesosphere (Livesey et al., 2020). Analyzed together, these two satellite datasets provide vertical coverage of CO from the surface to the mesosphere. HCN measured by the Atmospheric Chemistry Experiment Fourier Transform Spectrometer (ACE-FTS) instrument is also analyzed to further determine the influence of local biomass burning in the tropical stratosphere.

Using the Community Atmosphere Model with Chemistry (CAM-chem) state-of-the-art global chemistry climate model run with specified dynamics, we aim to understand how the CO is transported into the stratosphere during the fire event in 2015. The impact of the elevated CO from the fires after it is transported into the lower stratosphere is examined in terms of changes in CO after the event. Two model configurations with different fire emissions are compared to examine the impact of the fires on ozone in the lower stratosphere for October 2015. Changes in ozone can be attributed to both transport and chemistry in this region and detailed analysis of ozone is not included here. In addition, CO tracers that only include biomass burning emissions over specified source regions (tagged-CO) have been added to the CAM-chem simulations to allow the examination of transport pathways for CO emitted from wildfires in Indonesia during October–December 2015.

In the tropical upper troposphere, the temporal variation of CO is determined by variations in CO sources, deep convection, and the ascent rate associated with the Brewer-Dobson circulation (Duncan, Strahan, et al., 2007). In the tropical lower stratosphere, the temporal variation of CO is influenced by the stratospheric Quasi-Biennial Oscillation (QBO, see Baldwin et al., 2001), as well as the seasonal cycle (Park et al., 2013). To characterize the relative influence of the QBO, seasonal cycle and El Niño, we performed multiple linear regression analyses (e.g., Ziemke et al., 1997) on the CO monthly mean time series measured by MLS.

2. Satellite Data and Model Description

2.1. MOPITT

The MOPITT instrument is a multi-channel thermal infrared (TIR) and near-infrared (NIR) instrument on board the EOS-Terra satellite launched in 1999 into a sun-synchronous polar orbit with ~10:30 a.m. local time descending node equator crossing. MOPITT has horizontal spatial resolution around 22 × 22 km and a swath width around 640 km, which allows global coverage every 3 days. MOPITT uses gas-cell correlation radiometry (Drummond et al., 2010; Edwards et al., 1999; Tolton & Drummond, 1997) to detect atmospheric CO absorption at 4.6 μm (TIR channels) and 2.3 μm (NIR channels). MOPITT retrievals of the CO volume mixing ratio profile are performed for cloud-free observations and use optimal estimation (Deeter et al., 2011 and references therein) with a ten-layer vertical retrieval grid. The TIR observations rely on upwelling thermal radiance and are sensitive to the vertical profile of CO mostly in the free troposphere. NIR observations use reflected solar radiation over land to obtain a total column measurement. Combining TIR and NIR in a multispectral retrieval allows enhanced sensitivity to the near-surface layer of CO for daytime land scenes (Deeter et al., 2011; Worden et al., 2010). Here we use MOPITT version 8 monthly average Level

3 combined TIR and NIR retrievals (V8J) on a 1° latitude × 1° longitude grid. From V6 to V8, MOPITT has used a priori profiles gridded at 1.9° latitude × 2.5° longitude resolution, taken from a climatological 2000–2009 run of CAM-chem (Lamarque et al., 2012). Only CO profiles with Degrees of Freedom (DOF) larger than 0.75 are included in the analyses to exclude strong influence from the a priori (see Worden et al., 2013). MOPITT retrieval uncertainties, which include both smoothing error and retrieval noise, are highly variable depending on pressure levels (Deeter et al., 2019). MOPITT retrieval uncertainties are reported in the Level 2 product files. MOPITT retrievals require meteorological parameters such as atmospheric and surface temperatures and water vapor profiles. In V7 to V8, these are from the MERRA-2 reanalysis products (Modern-Era Retrospective analysis for Research Applications) (Gelaro et al., 2017). The major innovation of V8 (Deeter et al., 2019) is to correct temporal bias drifts with respect to in situ observations that were present in V7 (Deeter et al., 2017) and earlier at different profile layer pressures and that are likely due to slowly changing parameters within the MOPITT instrument. This correction is applied to MOPITT Level 1 radiances only and also accounts for biases with respect to water vapor (and therefore latitude). In V8, temporal bias drifts with respect to in situ observations are now within the errors of the validation comparisons. MOPITT V8 data are available at: https://eosweb.larc.nasa.gov/datapool.

2.2. MLS

The Microwave Limb Sounder (MLS) on board the Aura satellite was launched into a sun-synchronous near-circular polar orbit in July 2004 (Waters et al., 2006). MLS obtains global coverage from 82°S to 82°N on ∼15 orbits per day, resulting in ∼3,500 daily profiles. Here we use MLS CO Level 2 (L2) products based on version 4.2 (v4.2) retrieval algorithms (Livesey et al., 2020). The vertical resolution of MLS CO is in the range 3.5–5 km from the upper troposphere to the lower mesosphere and ∼5 km in the UTLS. The lowest level of the MLS data recommended for scientific analyses is 215 hPa. The horizontal resolution varies with altitude but is in the range 400–700 km in the region of interest. The systematic uncertainty in v4.2 MLS CO also depends on altitude, ranging from ±10% at 10 hPa to ±38 ppbv + ±30% at 215 hPa (see Livesey et al., 2020 for details). We construct daily gridded data on 7.5° × 15° (latitude × longitude) horizontal grids. Monthly mean data is constructed by averaging daily data each month from September 2004 to December 2019.

2.3. Atmospheric Chemistry Experiment Fourier Transform Spectrometer

The Atmospheric Chemistry Experiment Fourier Transform Spectrometer (ACE-FTS) on board the Canadian-led science satellite, SCISAT-1, was launched into a high-inclination (74°) low-Earth orbit (altitude 650 km) on August 12, 2003 (Bernath, 2017; Bernath et al., 2005). ACE-FTS collects solar occultation absorption measurements in the infrared (2.4–13.3 μm or 750 to 4,400 cm^{-1}) at high resolution (0.02 cm^{-1}) and provides vertical profiles of trace gas mixing ratios with vertical resolution of ∼3 km from the troposphere to the lower thermosphere (∼5–120 km). The vertical field of view of the instrument is ∼3 km and the retrieval results are provided on a standard 1 km vertical grid (Boone et al., 2005, 2013). Uncertainties of ACE-FTS CO version 2.2 are better than 15% in the upper troposphere (8–12 km) and better than 30% in the lower stratosphere (12–30 km, Clerbaux et al., 2008). We use ACE-FTS v4.1 measurements of CO and HCN (Boone et al., 2020; Sheese et al., 2017) from February 2004 to December 2019. Monthly mean data are constructed by combining all the available measurements within the latitude bands (see Park et al., 2013).

2.4. CAM-Chem

We use the CAM-chem, the atmospheric component of the Community Earth System Model Version 2 (CESM2; Danabasoglu et al., 2020), including comprehensive tropospheric and stratospheric chemistry, to simulate CO during the 2015 El Niño event. CAM-chem is coupled to the Community Land Model Version 5 (CLM5) and uses prescribed ocean and sea-ice for this study. This version of CAM-chem includes the updated gas-phase chemistry mechanism MOZART-T1, coupled to MAM4 (Modal Aerosol Model with 4 modes), and includes an updated representation of secondary organic aerosols (Emmons et al., 2020; Tilmes et al., 2019). Simulations are performed on 1.25° × 0.9° (longitude × latitude) horizontal grids and with 32 vertical layers. The anthropogenic emissions have been provided by Community Emissions Data System

(CEDS) for the Coupled Model Intercomparison Project Phase 6 (CMIP6, Hoesly et al., 2018). We use the anthropogenic emissions of 2014, which is the latest of the available years, repeated for 2015. Biogenic emissions are interactively calculated in CLM by using the Model of Emissions of Gases and Aerosols from Nature (MEGAN2.1) (Guenther et al., 2012). Greenhouse gas mixing ratios are prescribed at the surface based on observations and future climate scenarios (Meinshausen et al., 2017).

Biomass burning emissions are available daily from the Fire INventory from NCAR (FINN) version 1.5 (Wiedinmyer et al., 2011). The FINN biomass burning emissions have been used to simulate transnational transport of CO from the surface over the Malaysian peninsula in September and October 2015 using a regional model, WRF-chem (Mead et al., 2018). WRF-chem simulations with fires show closer agreement with the observations than the simulations without the fires (see Figure 2 of Mead et al., 2018). We also used the Quick Fire Emissions Data Set (QFED) version 2.5 (Darmenov & da Silva, 2015) in CAM-chem simulations for October 2015 and compared with the model simulations using FINN. Neither FINN nor QFED emissions inventories include peat fires (Kiely et al., 2019; Nechita-Banda et al., 2018). Top-down emissions estimates have large uncertainty and have the tendency to underestimate fire emissions due to difficulties in detecting small fires or fires with weak thermal signature, such as peat fires (Darmenov & da Silva, 2015; Kiely et al., 2019; Shi et al., 2019). For more information about explicit treatment of peatland burning, see van der Werf et al. (2010).

In the CAM-chem specified dynamics configuration used here, temperature, winds, and surface fluxes are nudged to the MERRA-2 reanalyses with a 50-h relaxation time. In the specified dynamics configuration, the chemical and aerosol distributions, including the pollution from the Indonesian wildfire, do not alter the dynamical field. MERRA-2 has been interpolated to the CAM-chem vertical grid. This allows the model to generate its own physical fields, such as clouds or convection, on its native grid without diverging from synoptic meteorology. For October–December 2015, an additional CO tracer emitted from biomass burning near the surface over Equatorial Asia including Indonesia (95–160°E, 10°S–6°N) is included in the simulation, and the model output is saved every 6 h.

We use the monthly mean thermal tropopause height is obtained from the National Center for Environmental Prediction/National Center for Atmospheric Research (NCEP/NCAR) reanalysis (Kistler et al., 2001) in conjunction with the satellite data.

3. Seasonal and Interannual Variability of CO in the Tropical Troposphere

In the tropical UTLS, sub-seasonal to interannual variations in CO are mainly controlled by surface emissions, local convection and large-scale circulation (e.g., Inness et al., 2015; Jiang et al., 2007; Liu et al., 2013; Park et al., 2013; Pommrich et al., 2014; Schoeberl et al., 2006). Large-scale climate variability in the tropical troposphere, such as El Niño, can have a significant impact on atmospheric circulation and convection and hence on the distribution of atmospheric CO (e.g., Chandra et al., 2009; Field et al., 2016; Huang et al., 2014; Nassar et al., 2009). Figure 1 shows time series of monthly mean zonal average CO in the Southern Hemisphere (SH) tropical upper troposphere obtained from the satellite instruments MOPITT, MLS, and ACE-FTS from 2004 to 2019. Monthly mean CO is averaged in the SH tropics to examine how the different instruments capture CO emissions from the biomass burning in the SH spring. For MOPITT CO, individual monthly mean data at each latitudinal grid point are shown as well as the overall average values in the latitude band in Figure 1. Monthly mean MLS CO data are also shown. For ACE-FTS, due to the limited number of measurements at low latitudes, all the available profiles within the latitude band are averaged for each month (see Park et al., 2013). The vertical levels selected for presentation in Figure 1 were chosen such that the measurements from all instruments are sampling roughly the same region, given their respective vertical resolutions. For instance, MOPITT CO at 300 hPa represents a layer average over the 300–200 hPa range, but with a broad averaging kernel, typical of nadir observations, that shows contributing information from the middle to upper troposphere (Deeter et al., 2004, 2019). The vertical averaging kernels of MLS CO at 215 hPa are peaked at that level, but with ~5 km vertical resolution, they have significant influence from the adjacent pressure levels (Livesey et al., 2020). ACE-FTS retrievals have no associated averaging kernels (Boone et al., 2005). Averages from this instrument are generated at 12.5 km from the CO profiles on the

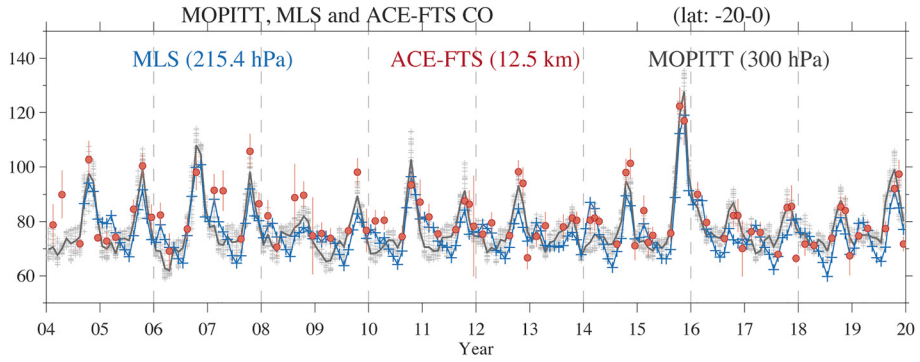

Figure 1. Time series of monthly mean CO mixing ratios (unit: ppbv) from MOPITT at 300 hPa (light gray plus signs and solid dark gray line), MLS at 215 hPa (blue solid line with plus signs), and ACE-FTS at 12.5 km (solid red dots) averaged from 20°S to the Equator. Red thin solid lines denote the 1-sigma standard deviation derived from the monthly averages of ACE-FTS CO. ACE-FTS, Atmospheric Chemistry Experiment Fourier Transform Spectrometer; MLS, Microwave Limb Sounder.

1-km altitude grid; the 12.5 km level is chosen because it is closest to ~215 hPa in the tropics for the United States Standard Atmosphere (Sissenwine et al., 1976).

The dominant variability in the CO time series shown in Figure 1 is the seasonal cycle, with maxima in October–November and minima in July. The CO maxima in October–November are due to large biomass burning emissions in tropical Asia, especially in Indonesia (Duncan, Martin, et al., 2003; Huang et al., 2014), and the CO minima in July are related to reactions with OH. There are small secondary peaks in both the MOPITT and MLS CO time series during Northern Hemisphere (NH) spring (March–April), which are related to biomass burning emissions in Southern Africa and Brazil (Duncan, Martin, et al., 2003) and also tropical convection (Duncan, Strahan, et al., 2007). The semi-annual oscillation is clear in MLS CO at 215 hPa. However, the smaller CO peak in NH spring is more prominent in the upper versus middle troposphere (Osman et al., 2016) and is not always captured by MOPITT due to its broader vertical resolution compared to the limb sounding instruments. In spite of the instrument's limited sampling, ACE-FTS also observes the seasonal maxima in the SH spring and minima in the NH summer. Thus all three instruments are able to capture the CO maxima in the SH upper troposphere due to increased surface emissions related to wildfires.

There is also significant interannual variability in the CO time series in Figure 1. The maximum CO mixing ratio for this time period was observed in the fall of 2015, and secondary maxima were observed in late 2006 and 2010; all were tied to strong El Niño events (Field et al., 2016; Huang et al., 2014; Mead et al., 2018; Ott et al., 2010; Santoso et al., 2017). In 2015, extreme biomass burning in Indonesia due to El Niño had a significant influence on air quality over the wider Equatorial Asian region; CO concentrations reached over 1,000 ppb due to wildfires near the surface during September—October 2015 (Mead et al., 2018). It is clear from Figure 1 that during strong El Niño events, like the one in 2015, CO in the tropical upper troposphere increases dramatically (up to ~140 ppbv) due to increased CO emissions near the surface.

Figure 2 shows the temporal variability of 5-day average CO from MOPITT in the mid-troposphere (500 hPa) and daily average CO from MLS in the upper troposphere (147 and 100 hPa) from July through December 2015. CO is averaged in the deep tropics (15°S–15°N) to examine large-scale changes related to transport processes. In the mid-troposphere (Figure 2a), MOPITT CO shows higher mixing ratios near Africa (0–40°E), Southeast Asia (60–120°E) and South America (60°W–0), which are closely related to local biomass burning emissions (Duncan, Martin, et al., 2003). The CO maximum located over Southeast Asia (60–120°E) has the highest values (>250 ppbv) from mid-September through November (Figure 2a). Wildfire emissions in Indonesia were most intense in September–October 2015 (Field et al., 2016; Mead et al., 2018). The MOPITT CO measurements at the surface indicate localized maxima from mid-September to mid-October in Indonesia (not shown), which is consistent with the in situ observations shown in Mead et al. (2018). MLS CO at 147 hPa (Figure 2b) shows maxima over Southeast Asia and South America that have different spatial distributions and cover wider geographical regions than those observed by MOPITT. Large-scale circulation plays a significant role in transporting pollutants from the surface into the upper troposphere

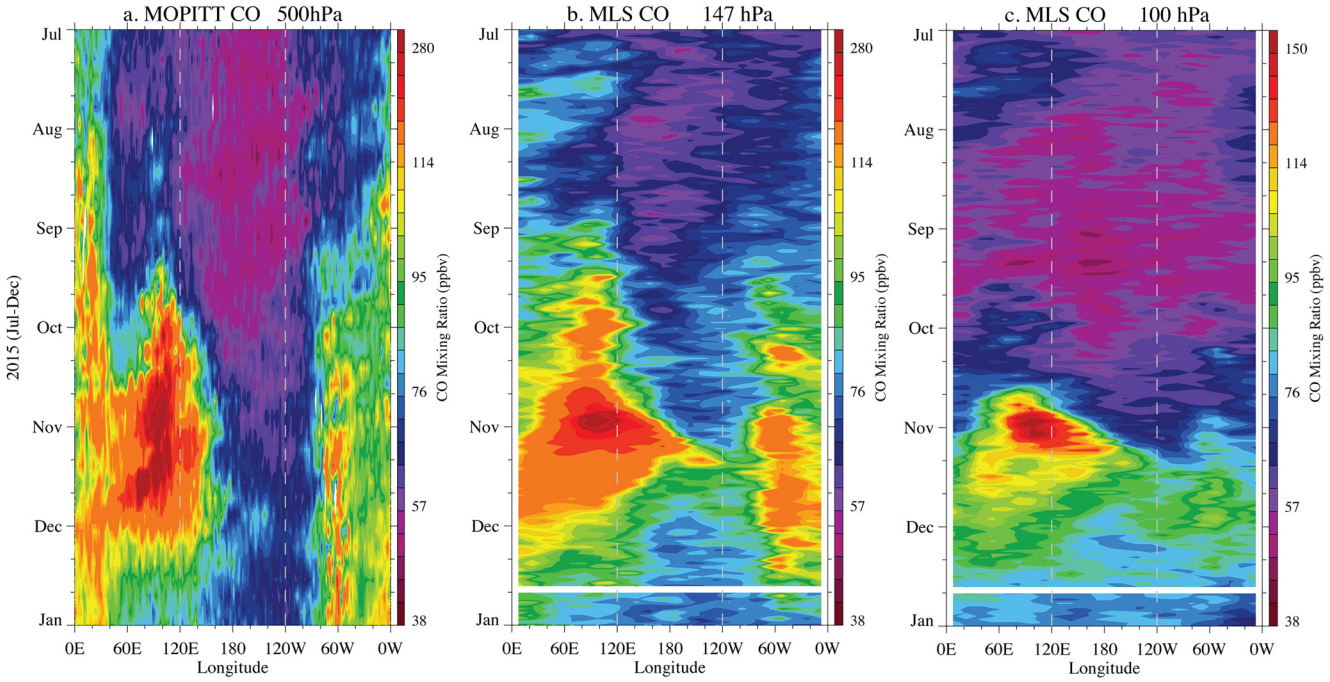

Figure 2. Hovmöller diagrams of MOPITT CO 5-day averages at 500 hPa (a) and MLS CO averaged each day at (b) 147 hPa, and (c) 100 hPa (unit: ppbv) between 15°S and 15°N latitude from July through December 2015. Note that a different color scale is used in Figures 2a–2c. MLS, Microwave Limb Sounder; MOPITT, Measurement of Pollution in the Troposphere.

(Mahlman, 1997; Duncan, Strahan, et al., 2007). The timing of widespread maxima seen in MLS CO coincides with the MOPITT CO maxima with different spatial structure, which indicates strong influence from large-scale transport. For instance, the CO maximum over Africa (0–40°E) in the upper troposphere at 147 hPa (Figure 2b) shows greater dispersion than the maximum at 500 hPa (Figure 2a). In addition, the timing of the maxima over Southeast Asia and South America differs from that in Figure 2a. The highest values in MLS CO appear in late October over Southeast Asia (60–120°E) and propagate to the east away from the source regions from mid-October to November. This quasi-horizontal transport is mainly driven by the subtropical jets, as shown in Duncan, Strahan, et al. (2007)'s modeling study for the 1997 El Niño event. The CO maxima related to the Indonesian wildfires (near 120°E) peak between mid-October and late November at 500 hPa (Figure 2a) and in early November at 147 hPa (Figure 2b). The lag in the timing of CO maxima at those two pressure levels suggests that the CO maximum at 147 hPa is influenced by large-scale slow vertical transport as well as surface emissions and convection (Jiang et al., 2007). This is consistent with the results of a global modeling study of ozone, which emphasized the role of large-scale transport after the fire activity related to the El Niño event in 2006 diminished in December (Chandra et al., 2009). MLS CO at 100 hPa (Figure 2c) shows a maximum in November over Southeast Asia (60–120°E) and a secondary maximum in mid-November near South America (60°W). An apparent time lag between the CO maxima at 147 and 100 hPa (Figures 2b–2c) over Indonesia indicates that slow vertical transport continues to play a role in transporting CO from the upper troposphere into the lower stratosphere. MLS data at 68 hPa suggest that CO is enhanced at all longitudes in late November and December (not shown). This zonally symmetric distribution in CO arises from symmetric horizontal circulation patterns in the tropical lower stratosphere (Wallace, 1973). We note that there is a hint of a time lag between the 215 and 100 hPa maxima in the MLS CO time series shown in Figure 2 of Field et al. (2016) that was not discussed in detail in their study. The role of vertical transport for CO originating from biomass burning is also shown by Pumphrey et al. (2011), who examined Australian wildfire emissions using MLS CO measurements. The recent 2019/20 Australian bushfires resulted in unprecedented perturbations to the dynamical circulation as well as the composition in the stratosphere (e.g., Khaykin et al., 2020 and Schwartz et al., 2020).

It has been shown that during El Niño events, tropical deep convection is shifted to the Eastern Pacific, where it is closer to the source regions over South America and contributes to the vertical transport of

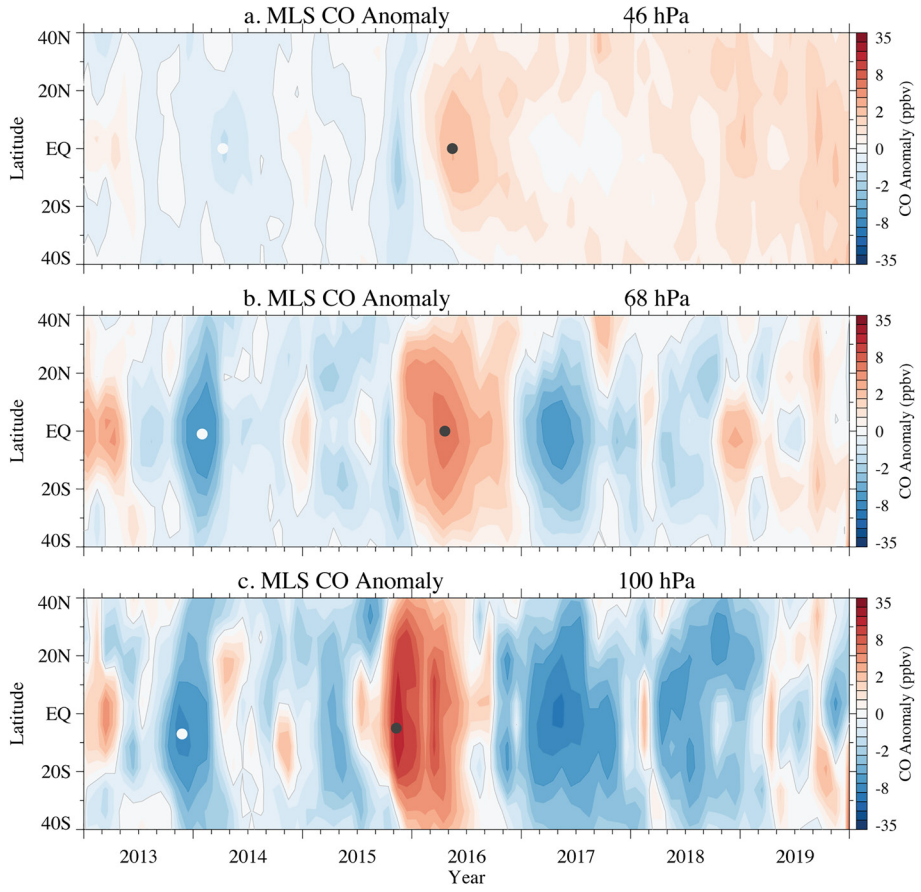

Figure 3. Time-latitude sections of monthly mean CO anomalies from MLS (unit: ppbv) at (a) 46 hPa, (b) 68 hPa, and (c) 100 hPa for 2013–2019. Note, contour intervals are non-linear to display both high values in the troposphere and low values in the stratosphere. White and black solid circles indicate the locations of the minima in 2013–2014 and the maxima in 2015–2016 at each pressure level, respectively. Solid light gray lines depict zero contours. MLS, Microwave Limb Sounder.

biomass burning trace gases and aerosols into the upper troposphere (Duncan, Strahan, et al., 2007; Ott et al., 2010). For the 2015 El Niño event, the largest upper tropospheric CO mixing ratios were observed over Southeast Asia in November, which is close to the Indonesian source region, and a secondary maximum is located over South America. The CO mixing ratios remained elevated in December 2015 at 147 and 100 hPa (Figures 2b–2c). Vertical transport of enhanced CO from the upper troposphere to the lower stratosphere is clearly shown in Figure 3. In Figure 3, we show monthly mean CO anomalies at three different pressure levels in the lower stratosphere (46, 68, and 100 hPa) obtained from MLS for 7 years starting in 2013. Monthly mean CO anomalies are constructed at each latitude grid point by removing the climatological seasonal cycle from monthly mean zonal averages at each pressure level. MLS CO anomalies at 100 hPa (Figure 3c) show negative values in late 2013 and 2017–2018 and a strong positive anomaly in late 2015, with a relatively weak positive anomaly in early 2016. CO anomalies at 68 hPa (Figure 3b) show two distinct negative periods in 2014 and 2017 and a distinct positive period in 2016. The positive anomaly in 2016 is persistent throughout the year, with a maximum occurring in April. The pollutants are transported further into the tropical lower stratosphere by slow ascent, especially over the Indian Ocean, and by quasi-horizontal mixing into the lowermost stratosphere. Both the CO maxima and minima at 68 hPa are centered at the Equator, with apparent time lags of ~3–6 months between the 100 and 68 hPa pressure levels. The apparent time lag between 100 and 68 hPa is related to the slow ascent playing a role in vertical transport of CO (see Duncan, Strahan, et al., 2007). Specifically, the CO minimum at 68 hPa appears ~3 months after the minimum appeared at 100 hPa in 2013–2014, and it takes up to ~6 months for the CO maximum at 100 hPa to reach 68 hPa in 2015–2016. The year-to-year variability in the timing of the CO minimum at 68 hPa reflects

interannual variability in ascent rates in the tropics (Schoeberl et al., 2008). The positive CO anomaly in 2016 lasts longer than the negative CO anomalies in 2013 and 2017 at 68 hPa (Figure 3b). Vertical transport of the minimum and the maximum CO continues to higher altitude in the stratosphere (46 hPa, Figure 3a). Transport of high CO from the tropics to the subtropics and mid-latitudes is obvious at 46 hPa, which shows a broader positive anomaly starting in early to mid-2016. At 46 hPa, the CO distribution is predominantly influenced by the large-scale meridional circulation and quasi-horizontal mixing (e.g., Baldwin et al., 2001; Duncan, Strahan, et al., 2007). The apparent increasing tendency in CO at 46 hPa in the latter half of the record (after 2016) requires further investigations beyond the scope of this study.

4. Transport of CO into the Stratosphere

Although the 2015 wildfire season in Indonesia ended in October (Field et al., 2016), anomalously high CO was observed in the tropical lower stratosphere in 2016 because of its relatively long residence time in the lower stratosphere (a few months) and large-scale transport (see Duncan, Strahan, et al., 2007). Given its relatively long chemical lifetime (about 3 months), the distribution of CO in this region is expected to depend strongly on meridional and vertical transport and throughout the middle atmosphere (Brasseur & Solomon, 2005). CO emitted from wildfires reaches maxima in the lower troposphere from mid-September to October as discussed in Section 3. In this section, the mechanisms for vertical transport of high CO emitted from the Indonesian wildfires into the tropical UTLS are discussed in detail. Previous studies have shown that vertical transport from the troposphere to the stratosphere occurs primarily in the tropics (Randel et al., 2007, 2010) through the upwelling branch of the Brewer-Dobson circulation (Butchart, 2014). Due to seasonal changes in temperature, there exists an annual cycle in the tropical upwelling, with maximum strength in NH winter (Abalos et al., 2015; Randel et al., 2007). Tracers with steep vertical gradients near the tropopause are affected by the seasonal changes in vertical velocity in the tropical UTLS. For instance, CO and O_3 show a strong seasonal cycle in their concentrations near the tropical tropopause (e.g., Park et al., 2013; Randel et al., 2007; Schoeberl et al., 2006). Local emissions and convection play an important role in seasonal changes in CO in the tropical upper troposphere (e.g., Schoeberl et al., 2006), and the surface emissions tend to have large year-to-year variation (e.g., Duncan, Martin, et al., 2003; van der Werf et al., 2010). The relative importance of CO emissions and the seasonal cycle in tropical upwelling is highlighted by Park et al. (2013), who show that in the tropical upper troposphere (up to 147 hPa), time series of CO display predominantly interannual variability, with the maximum in the fall of 2006 due to higher emissions during El Niño. In the lower stratosphere (68 hPa), an annual cycle in the CO time series, with the maximum in NH winter, is the dominant variability. At 100 hPa, the CO time series shows hints of both interannual variability and the annual cycle (Duncan, Strahan, et al., 2007; Park et al., 2013).

Another important dynamical influence on the vertical transport of CO in the tropical stratosphere is the stratospheric Quasi-Biennial Oscillation (QBO). The stratospheric QBO consists of downward propagating easterly and westerly regimes in the equatorial zonal winds with an average period of approximately 28 months (Baldwin et al., 2001). The QBO influence on long-lived tracers is exerted through the transport associated with the secondary meridional circulation tied to the zonal winds and temperature gradients in the tropical lower stratosphere (Holton & Tan, 1982; Baldwin et al., 2001). In order to focus on the interannual variation in CO, we show monthly mean CO anomalies obtained from MLS in the tropical upper troposphere and stratosphere (~200–10 hPa) in Figure 4. There exists large year-to-year variability in the CO anomalies, with positive anomalies below the tropopause associated with burning seasons in the tropics. Notably, high CO events in the upper troposphere in 2005, 2006, and 2015 are related to wildfires induced by El Niño (Logan et al., 2008; Nassar et al., 2009). These positive CO anomalies are transported into the stratosphere up to ~40–50 hPa, which is consistent with the "CO tape recorder" shown in Schoeberl et al. (2006, see their Figure 1). In the mid-stratosphere (above ~20 hPa), interannual variability in CO is influenced by the QBO in the tropical zonal winds. The amplitude of the CO anomalies associated with the QBO is much smaller in comparison to other tracers with sources in the stratosphere, for example, ozone (figure not shown). Between ~20 and 40 hPa (~27–22 km), where CO has a weak vertical gradient (Schoeberl et al., 2008), CO anomalies show more complicated temporal variability, which may reflect influence by vertical transport from the troposphere and also from higher in the stratosphere.

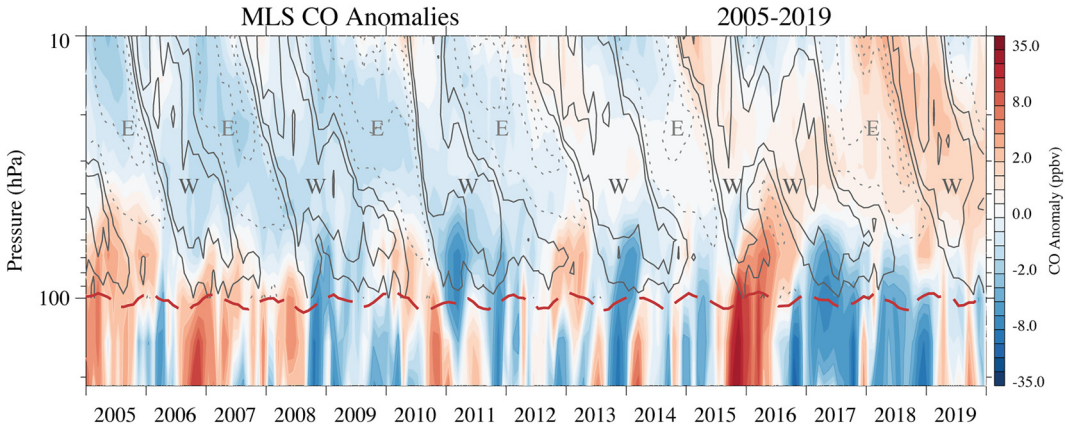

Figure 4. Time-pressure section of monthly mean CO anomalies from MLS (unit: ppbv) averaged between 15°S and 15°N latitude for 2005–2019. The same non-linear contour intervals used in Figure 3 are used here. Dark and light gray lines denote monthly mean zonal winds (unit: m/s) measured at Singapore (1°N/104°E). Solid lines represent westerly and dotted lines represent easterly wind, respectively. ±3 ppbv contours are added as blue (negative) and red (positive) solid contours. Monthly mean tropopause pressure (unit: hPa) obtained from the NCEP/NCAR reanalysis is shown as a red long dashed line. MLS, Microwave Limb Sounder.

The largest CO anomalies are apparent in the upper troposphere from the fall of 2015 to early 2016, and they continue to be transported into the stratosphere, reaching ~40 hPa (~24 km) by mid-2016. The magnitude and duration of these CO anomalies in the stratosphere are unprecedented in the Aura MLS record. Such large CO anomalies in the stratosphere had never been observed prior to December 2019, after which the impact of the CO emissions over Australia reached record stratospheric proportions in 2020 (Khaykin et al., 2020; Schwartz et al., 2020). In addition to the strong El Niño event in 2015, there was a disruption in the QBO phases in the stratosphere in 2016. Temporal variations in vertical velocity are influenced by interannual variations correlated to El Niño as well as QBO in the lower stratosphere (Minschwaner et al., 2016). It is possible that disruptions in the phases of the QBO may have contributed to the vertical transport of CO in 2016 (see Tweedy et al., 2017), and further investigation (beyond the scope of this study) is needed.

In order to examine the impact of biomass burning on CO variability in the stratosphere in more detail, we introduce HCN, which is produced almost entirely by biomass burning and has an additional chemical sink over the ocean surface (Li et al., 2000; Pumphrey et al., 2018; Singh et al., 2003 and references therein). HCN has a chemical lifetime of 5–6 months in the troposphere (Li et al., 2000) and up to a few years in the stratosphere (Kleinböhl et al., 2006; Glatthor et al., 2009), which makes it an ideal tracer to explore the transport from the troposphere into the stratosphere (Randel et al., 2010; Park et al., 2013; Glatthor et al., 2015; Pumphrey et al., 2018). In Figure 5, we show monthly mean mixing ratios of HCN obtained from the ACE-FTS instrument in the tropical stratosphere from 2005 through 2019. Despite the instrument's limited sampling in the tropics, ACE-FTS is able to capture the seasonal and interannual cycles in HCN (Park et al., 2013; Pumphrey et al., 2018). HCN mixing ratios in the troposphere show a seasonal cycle with maxima in the fall (Figure 5). The annual maximum value of HCN varies from year to year, with relatively higher values in 2006 and 2007. In the fall of 2006, CO anomalies are also higher than typical in the upper troposphere (Figures 1 and 4), which is likely related to El Niño. The distinct seasonal cycle in HCN is different from that in CO due to its longer chemical lifetime in the stratosphere.

In the fall of 2015, HCN mixing ratios show the highest values in the entire ACE-FTS record, persisting into the stratosphere for almost 2 years (2016–2017). The slope of the high HCN mixing ratios changes with altitude, which suggests faster vertical transport between ~90 to ~50 hPa (18–~22 km) and slower transport above ~23 km altitude. This undisturbed vertical transport of high HCN is consistent with the "HCN tape recorder" in the tropical stratosphere (Glatthor et al., 2015; Pommrich et al., 2010; Pumphrey et al., 2008). Pumphrey et al. (2008) suggested that, unlike the water vapor tape recorder, the HCN tape recorder signal appears to have an approximately 2-year cycle possibly influenced by interannual variations in biomass burning in Indonesia and the surrounding region. Pommrich et al. (2010) showed that the biomass burning in Indonesia plays an important role in the HCN tape recorder signal using Lagrangian model

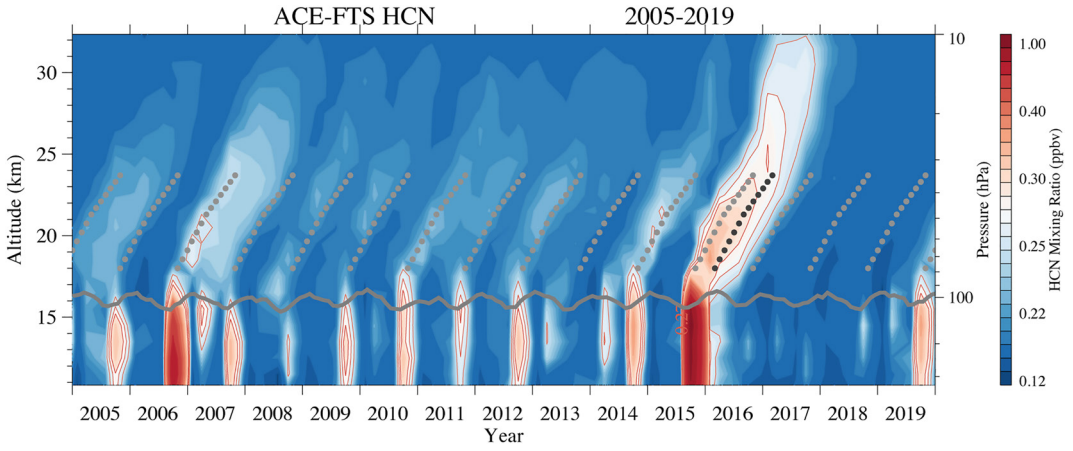

Figure 5. Time-altitude section of monthly mean HCN mixing ratios from ACE-FTS [unit: ppbv] averaged between 15°S and 15°N latitude for 2005–2019. Gray solid dots represent vertical velocity estimated based on Mote et al. (1996) with the tape recorder head placed in October each year. Black solid dots indicate tape recorder signal starting in February 2016 (see text for details). Red solid contours are added to mark high HCN mixing ratios (0.25, 0.27, and 0.29 ppbv). Monthly mean tropopause height obtained from the NCEP/NCAR reanalysis (unit: km) is shown as a thick gray solid line. ACE-FTS, Atmospheric Chemistry Experiment Fourier Transform Spectrometer; HCN, hydrogen cyanide.

simulations. Based on MIPAS observations, Glatthor et al. (2015) demonstrated that the HCN tape recorder has an annual cycle similar to that of water vapor. Figure 5 suggests that the temporal variability in HCN in the stratosphere is mainly seasonal, directly following the annual maximum values in the troposphere. There is large year-to-year variability in the maximum HCN values in the stratosphere. In autumn 2006, HCN values are high enough to affect the seasonal cycle of the following year (2007). As noted above, after autumn 2015, anomalously high HCN in the troposphere is transported into the stratosphere up to ~10 hPa (~32 km) over almost 2 years.

Here we performed a simple experiment with the monthly mean data to test the vertical transport of HCN in the tropical stratosphere. We applied the altitude-dependent vertical velocity estimated from the water vapor tape recorder shown in Mote et al. (1996). In Mote et al. (1996), the water vapor tape recorder signal propagates faster between 100 and 50 hPa (0.18–0.23 hPa/day) and slower above (50–20 hPa, 0.05–0.06 hPa/day). In our experiment, we did not consider interannual variability in the vertical velocity in the stratosphere as shown by Flury et al. (2013). Here, instead of placing the base of the tape recorder (the "tape head") at the cold point tropopause in NH winter (February), as is done for water vapor, the HCN tape head was placed at 18.5 km in NH fall (October) each year. The selection of those specific months is coincident with the limited sampling of ACE-FTS in the tropics (see Park et al., 2013). It is obvious from Figure 5 that high HCN due to local biomass burning enters the stratosphere every October. The vertical velocity estimates based on the water vapor tape recorder (shown as gray solid dots in Figure 5) are roughly consistent with the rate of the vertical propagation of high HCN into the stratosphere in October each year. Relatively higher mixing ratios of HCN entering the stratosphere each year persist into the following year. This is especially true for the 2005–2007 time period, when HCN seems to have a tape recorder signal with a 2-year cycle (Pumphrey et al., 2008). However, the entire data record instead suggests that the HCN tape recorder has an annual cycle, not a 2-year period, and that its amplitude varies substantially from year to year depending on the concentrations in the troposphere, as suggested by Pommrich et al. (2010) and Glatthor et al. (2015).

Anomalously high HCN in the troposphere linked to the wildfires in Indonesia in October 2015 extends well into the stratosphere in 2016 and 2017. The water vapor tape recorder for 2016 with the tape head placed at 18.5 km in February (shown as black solid dots in Figure 5) overlaps with the higher HCN mixing ratios that began in 2015. Using ACE-FTS measurements, Sheese et al. (2017) show elevated HCN abundances in the stratosphere through 2016 due to El Niño-driven fires in Indonesia in 2015. The daily mean HCN concentrations in the lower stratosphere were greater than the climatological mean (by 10%–90%) in 2016. Using MLS HCN measurements, Pumphrey et al. (2018) also show El Niño-induced elevated HCN in the stratosphere in 2016. With the extension of the data record, it is obvious (Figure 5) that enhanced

HCN at higher altitudes persisted through 2017, much longer than what has been shown previously. The persistence of high HCN in the stratosphere throughout 2017 suggests that not only did the 2015 fire emissions affect the troposphere, but they also had a 2-year impact on the stratosphere, which is unprecedented in the satellite record. Due to the long chemical lifetime of HCN in the stratosphere (Glatthor et al., 2009; Kleinböhl et al., 2006), El Niño conditions can have a significant impact on the HCN budget in the lower stratosphere; enhanced HCN can then be transported to higher latitudes (see Sheese et al., 2017).

5. Sources of CO Interannual Variability

As shown in the previous sections, local biomass burning emissions strongly influence the amount of CO transported into the stratosphere. In addition, atmospheric variability including the QBO and annual cycle can have a large impact on the variability in the transport in the tropical UTLS (Minschwaner et al., 2016). To quantitatively assess the impact of each source of variability on CO in the upper troposphere, we performed multiple linear regression analysis (e.g., Ziemke et al., 1997) using the monthly mean CO time series from MLS at 147 hPa. As the 147 hPa pressure surface lies below the tropopause, the influence of the QBO is not expected to be significant. Instead, dynamical variability in both the troposphere and stratosphere can alter the vertical transport indirectly as shown in Minschwaner et al. (2016). Also, modes of climate variability such as ENSO and QBO are not completely independent (Domeisen et al., 2019). Following Ziemke et al. (1997), the general regression model used here is

$$\Omega(t) = \alpha + \beta t + \gamma_1 \mathrm{QBO}_1(t) + \gamma_2 \mathrm{QBO}_2(t) + \delta\,\mathrm{solar}(t) + \varepsilon\,\mathrm{ENSO}(t) + R(t) \quad (1)$$

Here, Ω is CO time series,t is the time index with monthly time steps. α, β, γ_1, γ_2, δ, and ε are time-dependent regression coefficients given by a constant plus 12-month, 6-month, and 4-month cosine and sine harmonic series as defined by Randel and Cobb (1994). α represents the seasonal fit, β is the trend coefficient, and γ_1 and γ_2 are the QBO1 and QBO2 coefficients, respectively. δ is the solar flux series coefficient, and ε represents the El Niño coefficient. $R(t)$ is the residual time series. The QBO1 and QBO2 proxies are constructed based on the method shown in Wallace et al. (1993) using the monthly mean zonal winds observed at Singapore (Naujokat, 1986) for 2005–2019. The QBO1 and QBO2 proxies are defined by the coefficients of two leading empirical orthogonal functions (EOFs) at seven pressure levels over 70–10 hPa. These QBO proxies represent vertical structure of the QBO in the entire stratosphere instead of variability at a single pressure level (see also Ziemke et al., 1997; Park et al., 2017). The Multivariate El Niño and Southern Oscillation (ENSO) index (MEI, Wolter & Timlin, 1993) is used as a proxy for El Niño and is downloaded from NOAA Earth System Research Laboratory (https://www.esrl.noaa.gov/psd/enso/mei/). The seasonal dependency of each proxy is represented by a harmonic expansion with a constant and three harmonic terms as explained in Randel and Cobb (1994). As the wildfire activity in Indonesia has a strong positive correlation with ENSO (e.g., Field et al., 2016), we did not consider a time series of fire events in this calculation. The solar flux data averaged over each month are used as a proxy for the 11-year solar cycle (ftp://ftp.seismo.nrcan.gc.ca/spaceweather/solar_flux/monthly_averages/solflux_monthly_average.txt). Solar cycle influences on stratospheric ozone have been shown to be significant in the tropical lower stratosphere based on an analysis using long-term satellite measurements (Soukharev & Hood, 2006). Due to the relatively short data record, the solar cycle influence on the MLS CO time series is not significant in our study (not shown).

Figure 6 displays monthly mean anomalies, QBO1, QBO2, and ENSO regression fits to focus on the interannual variability. The seasonal cycle regression coefficient (α in Equation 1) has the largest amplitude, and the rest of the regression fits, including the solar cycle, trend and residual, have negligible contributions (not shown). The time series of CO anomalies (Figure 6a, top) shows relatively small positive and negative values until the maximum value appears in January 2016. The CO anomaly in January 2016 is almost three times larger than the rest of the monthly anomalies. This result shows that the anomalously high CO in the lower and middle troposphere in October 2015 being transported into the upper troposphere with positive time lags (Figures 2–5). The QBO1 and QBO2 regression fits are nearly orthogonal to one another and show relatively small contributions to CO anomalies (Figure 6a, middle). The QBO contribution to CO anomalies increases with altitude as the amplitude of the QBO increases in the lower stratosphere (not shown).

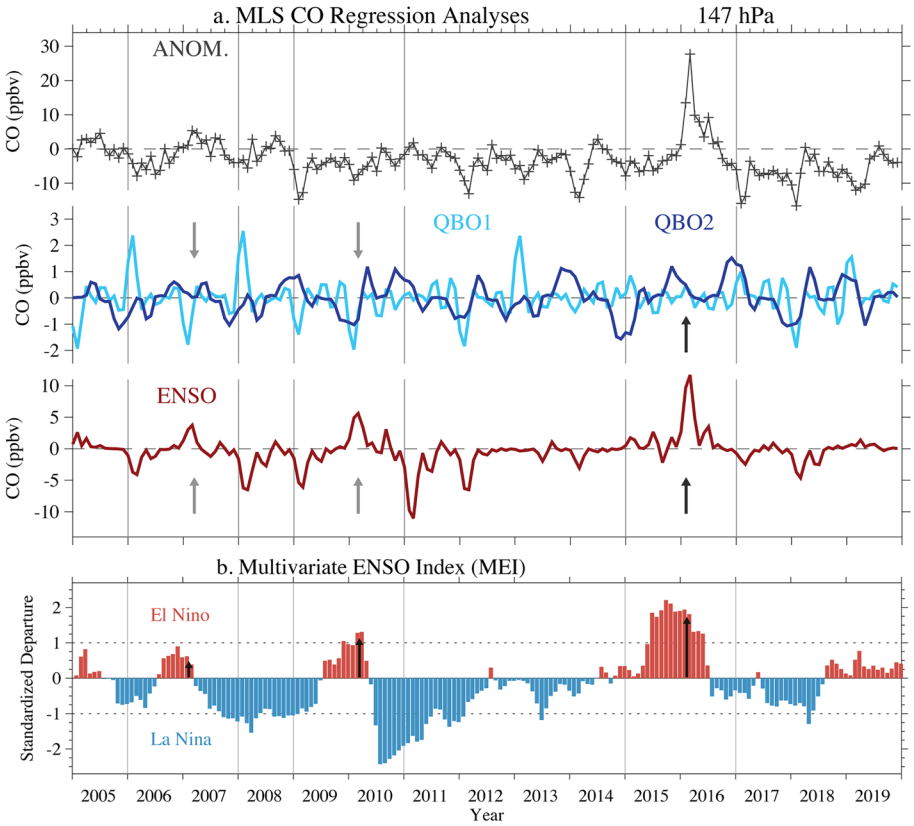

Figure 6. (a) Time series of monthly mean CO anomalies obtained from MLS (unit: ppbv) at 147 hPa averaged between 15°S and 15°N latitude (black). Multiple linear regression fits of QBO1 (solid light blue), QBO2 (solid dark blue), and ENSO (red solid line) to deseasonalized CO time series (b) Multivariate ENSO index (MEI) for 2005–2019 (https://www.esrl.noaa.gov/psd/enso/mei). Thin gray lines indicate three major El Niño events, 2006–2007, 2009–2010, and 2015–2016. Gray arrows indicate the two El Niño events that have positive influence from ENSO and negative influence from QBO (2006–2007 and 2009–2010). The black arrows indicate the 2015–2016 El Niño event showing positive influences from both ENSO and QBO. ENSO, El Niño and Southern Oscillation; MLS, Microwave Limb Sounder; QBO, Quasi-Biennial Oscillation.

The ENSO regression fits have larger amplitudes than the QBO fits (Figure 6a, bottom). The ENSO contribution to CO anomalies is positive during El Niño and negative during La Niña. During El Niño, both increased emissions and stronger convection may contribute to higher CO mixing ratios in the tropical upper troposphere (Field et al., 2016; Logan et al., 2008; Nassar et al., 2009). Monthly MEI for the same period (Figure 6b) indicates that there have been three major El Niño events since 2005, which are marked as gray and black arrows in Figures 6a and 6b. The typical duration of ENSO events is 9–12 months, and some events can last up to a few years (https://www.pmel.noaa.gov/elnino). El Niño events in 2006 and 2009 seemed to last for about 1 year, and the 2015 El Niño lasted for more than 2 years (Figure 6b). Not only was the duration of the 2015–2016 El Niño event longer than that of the previous events, but also the MEI was almost twice as large as the values for the other years. ENSO regression fits to monthly CO anomalies show maxima in January (Figure 6a) for the 2006–2007, 2009–2010, and 2015–2016 El Niño events (Figure 6b). The MLS 147 hPa CO anomalies show maxima in January instead of October, when the emission was higher near the surface due to strong El Niño. For the 2009–2010 El Niño event, CO anomalies are negative in January, when the influence from the QBO is stronger.

For the 2015 event, the positive CO maximum may arise from positive contributions from not only the strong El Niño but also the QBO, as the regression fits from ENSO and, in particular, QBO2 have the same positive sign. However, for the 2006 and 2009 El Niño events, the QBO1 and QBO2 regression fits have the opposite sign to the ENSO regression fit. In 2006, QBO1 has a strong negative contribution, and in 2009, both QBO1 and QBO2 have the same negative sign. The positive contribution to CO mixing ratios results

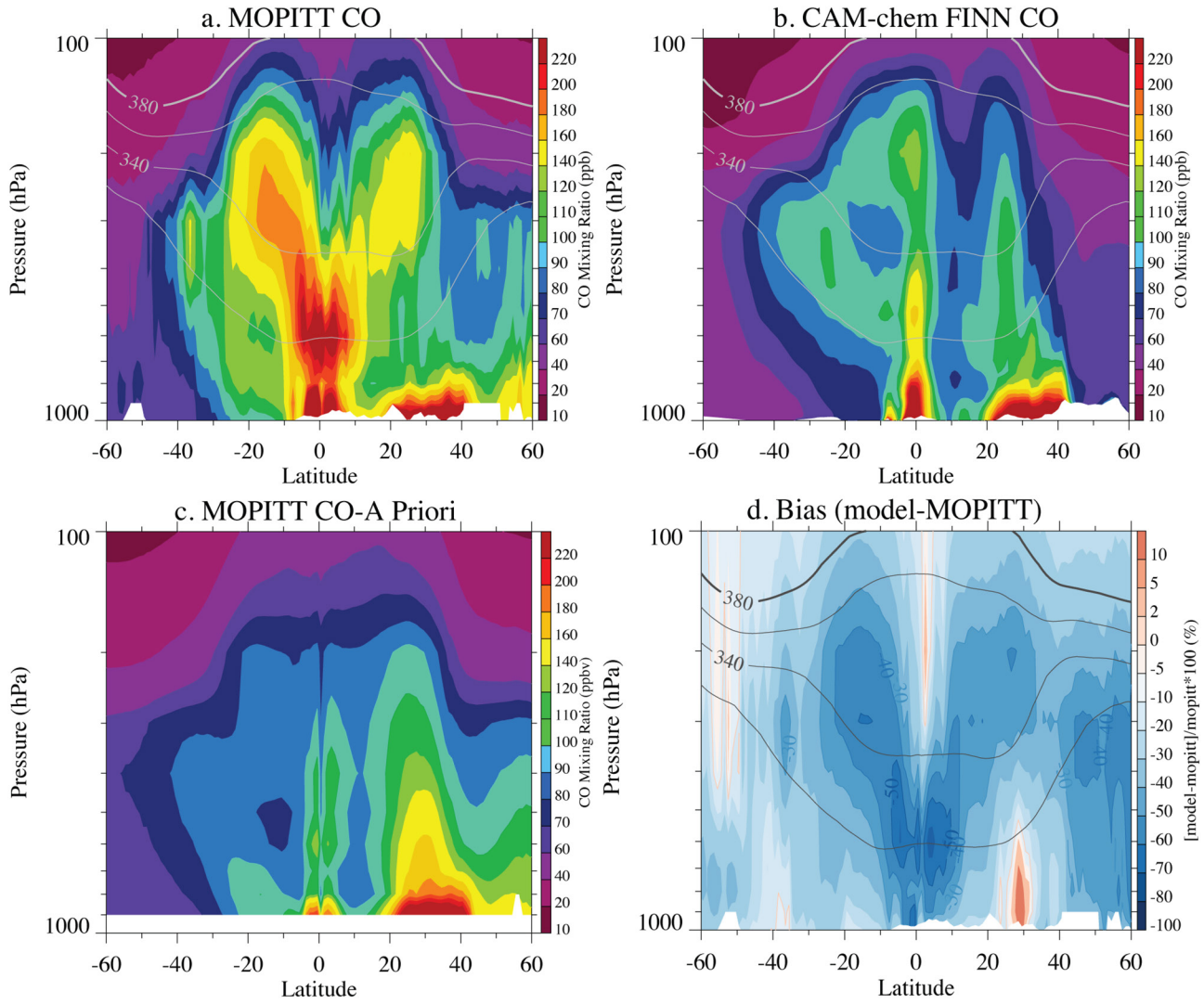

Figure 7. Latitude-altitude sections of monthly mean CO (a) from MOPITT V8J, (b) CAM-chem simulations after applying MOPITT sampling, averaging kernels and a priori, (c) CO a priori in the MOPITT retrievals, and (d) bias ((model-MOPITT)/MOPITT) × 100 (%) averaged between 110–120°E longitude for October 2015 (unit: ppbv). Gray solid lines denote isentropes calculated from the CAM-chem monthly mean temperatures. CAM-chem, Community Atmosphere Model with Chemistry; MOPITT, Measurement of Pollution in the Troposphere.

from the westerly phase of the QBO in the lower stratosphere (not shown). Recently, Diallo et al. (2018) found negative anomalies in O_3 and positive anomalies in H_2O as a result of the alignment of the 2015 El Niño and the QBO disruption using MLS observations and a Lagrangian transport model. In contrast to the results of Diallo et al., in our study, it is unclear whether the QBO disruption in 2015–2016 (e.g., Osprey et al., 2016; Tweedy et al., 2017) played a significant role in the positive CO anomalies at 147 hPa, as the amplitude of the QBO regression fit is relatively small (Figure 6a).

6. CAM-Chem Simulations of CO

In Figure 7, we compare monthly mean global CO distributions from MOPITT and CAM-chem simulations over Indonesia for October 2015. MOPITT CO shows an enhancement in the tropical lower to mid-troposphere up to ~400 hPa, which is related to emissions from wildfires over Indonesia (Figure 7a). In the upper troposphere, CO maxima are located in the subtropics between ~300 and 150 hPa in both hemispheres. The altitude of maximum CO in the upper troposphere coincides with the level of main convective outflow of ~200 hPa in the tropics (Folkins et al., 2000). This broad distribution of increased CO in the upper

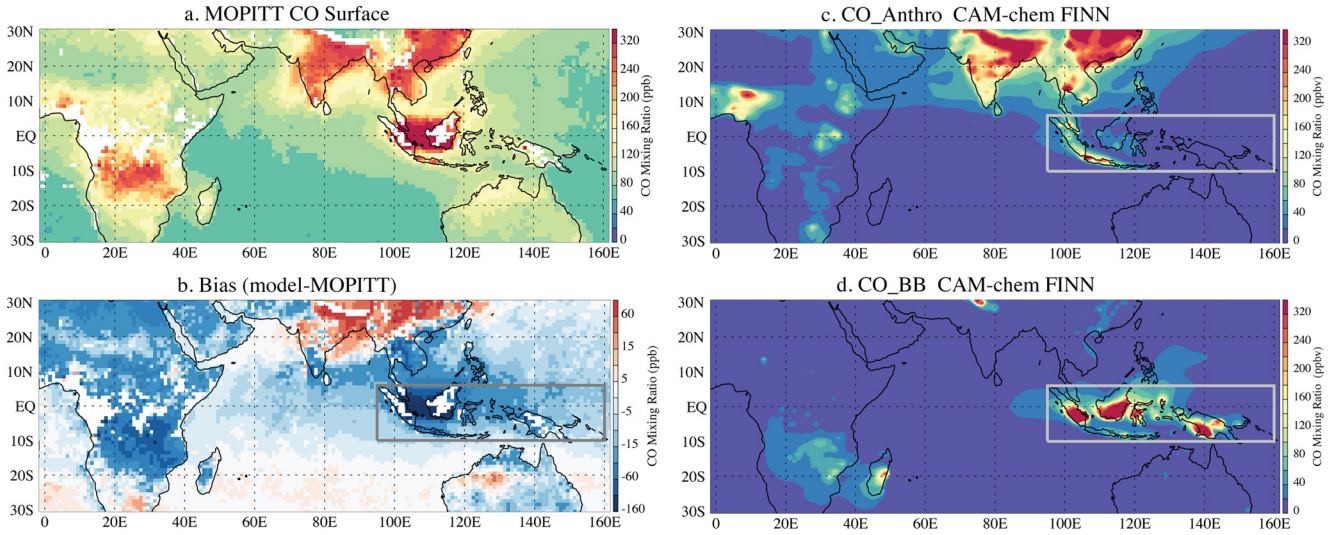

Figure 8. Monthly mean (a) CO mixing ratios at the surface from MOPITT and (b) bias (model-MOPITT), (c) anthropogenic emissions and (d) biomass burning emissions of CO from FINN for October 2015 (unit: ppbv). Enclosed boxes in Figures (b–d) represent the Equatorial Asia (EqAsia) region used in CAM-chem tagged-CO simulations (see Figures 9 and 10 for details). CAM-chem, Community Atmosphere Model with Chemistry; FINN, Fire INventory from NCAR; MOPITT, Measurement of Pollution in the Troposphere.

troposphere indicates that the influence of high CO emissions near the surface can be spatially more extensive at higher altitude due to its relatively long photochemical lifetime and large-scale transport. Note that because MOPITT retrievals are only performed under clear-sky conditions, CO mixing ratios from MOPITT in the tropical upper troposphere, where cloudy conditions prevail, are often under-sampled. Due to frequent cloud cover over Indonesia, it is likely that high CO concentrations near the equator are missed by MOPITT, whereas high CO is observed in the upper troposphere in transport regions away from the fire sources (Nechita-Banda et al., 2018).

CAM-chem simulations of CO for the same month (Figure 7b) show different features, with high CO near the surface in the tropics up to ~700 hPa and relatively weak maxima compared to MOPITT in the mid-troposphere for both hemispheres. We show the CO a priori in the MOPITT retrievals in Figure 7c. The CO maxima between 20–40°N latitude below ~700 hPa are related to anthropogenic emissions, not wildfires. At higher altitudes, the CO maxima in the measurements bear little resemblance to the a priori, confirming MOPITT measurement sensitivity to the fire emissions. In Figure 7d we show relative differences between CAM-chem and MOPITT monthly mean CO mixing ratios. For this comparison, MOPITT averaging kernels are applied to the model outputs and the difference is shown in percent (%). The difference between MOPITT and CAM-chem CO in Figure 7d highlights two main regions where CAM-chem CO is lower than that measured by MOPITT in October 2015: the tropical lower to mid-troposphere, and the subtropical (25°S–25°N) upper troposphere, where the level of main convective outflow is situated. There are also regions where CAM-chem overestimates CO, such as the NH midlatitude lower troposphere, narrow regions in the tropical upper troposphere, and the SH high latitudes (~60°S), which could be related to anthropogenic CO sources or transport.

The combination of surface emissions, convection and transport determines CO concentrations in CAM-chem in the troposphere. For instance, Huang et al. (2016) showed that global models underestimate CO in the UTLS region (215–100 hPa) compared to the MLS measurements and emphasized the role of surface emissions, convection and transport in determining global CO variability.

Fire activity over Indonesia has a seasonal cycle with maxima in September–October (e.g., Giglio et al., 2006) and also exhibits large interannual variability (van der Werf et al., 2006, 2017). Fire activity over Southern Africa and Southeast Asia also has a strong seasonal cycle, with peak biomass burning in NH winter and spring, respectively (Giglio et al., 2006; Wiedinmyer et al., 2011). In Figures 8a and 8b, surface CO mixing ratios from CAM-chem simulations are compared with the monthly mean CO from MOPITT to quantitatively

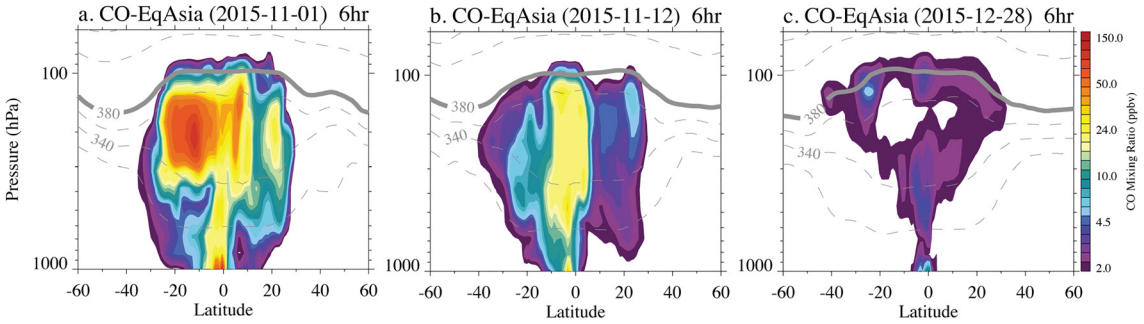

Figure 9. Latitude-altitude sections of tagged-CO simulations from CAM-chem averaged over 100–120°E longitude (unit: ppbv) for (a) November 1, (b) November 12, and (c) December 28. Thin dashed lines denote isentropes (unit: K), and the 380 K isentropic surface is shown as a thick solid line as a proxy for the local tropopause. CAM-chem, Community Atmosphere Model with Chemistry.

evaluate CO emissions included in the model for October 2015. MOPITT averaging kernels are applied to the CAM-chem CO to calculate the bias between the model and MOPITT in Figure 8b. Highest CO mixing ratios are observed over Indonesia (>260 ppbv), and secondary maxima exist in Southern Africa and Southeast Asia. Differences between CAM-chem and MOPITT surface CO mixing ratios (Figure 8b) suggest that CAM-chem underestimates CO over Indonesia, Australia and Southern Africa by up to ~50% (>160 ppbv over Indonesia) and overestimates CO over Southeast Asia by up to ~60%. It has been shown that global chemistry transport models tend to have systematic low biases in CO (Duncan, Logan, et al., 2007; Huang et al., 2014; Huijnen et al., 2019; Stein et al., 2014). The CO surface emissions included in the model have both anthropogenic and biomass burning sources (Wiedinmyer et al., 2011). In Figures 8c and 8d, we separate CO surface emissions from anthropogenic (Figure 8c) and biomass burning (Figure 8d) sources as included in the FINN emissions inventory. Over Southeast Asia, anthropogenic emissions contribute to higher CO in the model than indicated by the MOPITT measurements. The underestimation of CO over Indonesia in the model is mainly due to underestimation in biomass burning emissions (Figure 8d). This is related to the fact that wildfires in Indonesia burn a higher proportion of peat, which is not included in the inventories (Kiely et al., 2019). Sumatra and Kalimantan are known as the world's largest areas of tropical peatland (Harrison et al., 2009). Peatland forests experience smoldering fires, which produce high levels of carbon emissions and can last for weeks to months (e.g., Andreae & Merlet, 2001; Lohberger et al., 2018; Page & Hooijer, 2016; Page et al., 2002; Tansey et al., 2008). The smoldering fires of a peatland ecosystem are one of the hardest for the MODIS sensor to recognize (Sayer et al., 2014; Shi et al., 2019; Siegert et al., 2004), which can contribute to larger uncertainties in fire emissions estimates. Recent studies show that peat fires emit up to four times more CO than savanna and grassland and twice as much as boreal forest fires (Andreae, 2019). The omission of peat fires from the FINN inventory likely contributed to the modeled underestimation of fire emissions over Indonesia.

Even though the model underestimates the CO at the surface and in the tropical and subtropical troposphere in October, the monthly mean CO from both MOPITT and CAM-chem shows enhancement in the upper troposphere in November and December 2015, after the intense fire season ended in Indonesia (not shown). Based on the satellite observations, high CO emitted near the surface from wildfires is vertically transported into the lower stratosphere by December 2015 (see Section 4). In Figure 9, we show snapshots of CO from the tagged CAM-chem simulations (tagged-CO) for October-December to show the transport pathways of CO entering the stratosphere in CAM-chem. Note, CO-EqAsia represents CO emitted near the surface in Equatorial Asia (95–160°E/10°S–6°N), which includes Indonesia, to focus on the impact of Indonesian fires (see Figures 8b–8d). The dates and specific time steps in Figure 9 are chosen to best illustrate the vertical transport processes of tagged-CO during this time period. High concentrations of tagged-CO exist mostly in the tropics in October and can reach up to the tropical tropopause by end of the month (not shown). Once the fire activity starts diminishing in November, CO concentrations start decreasing near the surface but remain elevated in the wider regions of the tropical upper troposphere, as shown in Figure 9a for November 1. As in the monthly mean CO measurements from MOPITT (Figure 7a), CO concentrations in the tagged CAM-chem simulations are higher in the SH than in the NH. This hemispheric asymmetry seems to be stronger in the tagged-CO from the model simulations. By November 12 (Figure 9b),

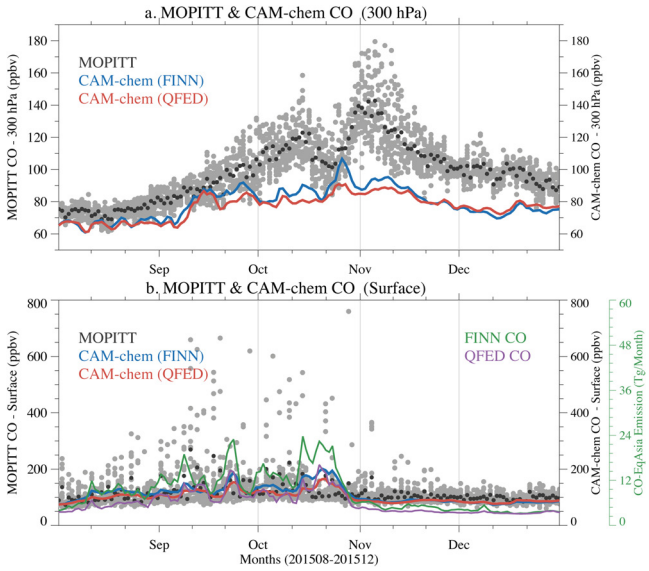

Figure 10. (a) Time series of daily CO mixing ratios (unit: ppbv) from individual MOPITT measurements (gray solid dots) at each grid point and mean values (black solid dots) over EqAsia (95–160°E and 10°S–6°S) for September–December 2015 at 300 hPa. Daily mean CAM-chem simulations are shown as blue (FINN) and red (QFED) solid lines. (b) Same as (a) but for the CO mixing ratios at the surface (unit: ppbv). Total CO emissions from FINN and QFED are added as green and purple solid lines, respectively, in (b). *Y*-axis on the right (green) corresponds to total CO emissions from both inventories (unit: Tg/Month). CAM-chem, Community Atmosphere Model with Chemistry; FINN, Fire INventory from NCAR; MOPITT, Measurement of Pollution in the Troposphere; QFED, Quick Fire Emissions Data Set.

the maximum CO concentrations in the troposphere have decreased by about ~50% compared to Figure 9a but still remain relatively high in the mid to upper troposphere in the SH. Also, the secondary maximum in the NH subtropical (near 20°N) upper troposphere remains elevated. It is not clear if the increased CO in the NH subtropics is directly related to the high CO in the SH. Further sensitivity tests are warranted to explore transport pathways leading to the CO maxima in the NH subtropical upper troposphere using tagged tracers with longer lifetime, but they are beyond the scope of this study. By December 28 (Figure 9c), remnants of elevated CO are still visible in the tropical troposphere and in the wider latitude regions in the lower stratosphere (reaching above the 380K isentropic surface). This suggests that CO is vertically transported into the stratosphere through the tropics and then transported towards higher latitudes. Once CO enters the stratosphere in December 2015, it is further transported to higher altitudes in January and February (not shown).

In Figures 8 and 9, we showed that high CO emitted from wildfires persists in the troposphere for over three months and is ultimately transported into the stratosphere due to its relatively long residence time in the UTLS (Nechita-Banda et al., 2018). In Figure 8, we showed that the CAM-chem simulations based on the FINN surface emissions underestimate CO compared to the MOPITT measurements for October 2015. To quantitatively compare not only the amount of CO but also the temporal evolution of CO emitted during the fire season, we show time series of daily CO from MOPITT and the CAM-chem simulations for August–December 2015 at the surface (Figure 10b) and in the upper troposphere (Figure 10a). In addition to the model simulations based on CO emissions from FINN, we included a CAM-chem simulation with surface emissions from QFED for the same period (Figures 10a and 10b). These two model simulations have the same configuration, so the only difference between the two is the surface emissions. We also included the total monthly emissions of CO (Tg/month) from FINN and QFED in Figure 10b. As noted above, a geographical region including Indonesia and Papua is chosen (EqAsia, 95°–160°E/10°S–6°N) to represent wildfire activity throughout the season and also to compare with the results from Nechita-Banda et al. (2018, see their Figures 4 and 5).

Estimates of CO surface emissions from QFED (Darmenov & da Silva, 2015) are slightly lower than those from FINN over EqAsia for September–October 2015 (map not shown here). This is reflected in the time series of CO emissions in Figure 10b. CO emissions from QFED have similar temporal evolution as those from FINN, with higher emissions in late September and October. The evolution of total CO emissions over EqAsia estimated from FINN and QFED is consistent with that of the prior Global Fire Assimilation System (GFAS) emissions presented in Nechita-Banda et al. (2018). Consequently, the CO surface mixing ratios from the CAM-chem simulations with both FINN and QFED emissions are generally lower than the daily CO measurements from MOPITT (Figure 10b). However, monthly mean MOPITT CO values are slightly lower than the CAM-chem simulations in late October in the region. The difference between the CAM-chem simulations and MOPITT maxima can be up to a factor of four when the CO mixing ratios are high. Note, the CO maxima in October are comparable to the ones in September in the model and the measurements at the surface, which is consistent with the results of Mead et al. (2018) and Nechita-Banda et al. (2018). In the upper troposphere (300 hPa), the daily time series of CO from MOPITT shows maxima in October and November (Figure 10a). The CO mixing ratios in December are higher than the values in August, before the fire season started. CAM-chem simulations of CO are lower than the MOPITT measurements from September to December by up to a factor of two, and the timing of CO maxima is earlier than those in the MOPITT time series.

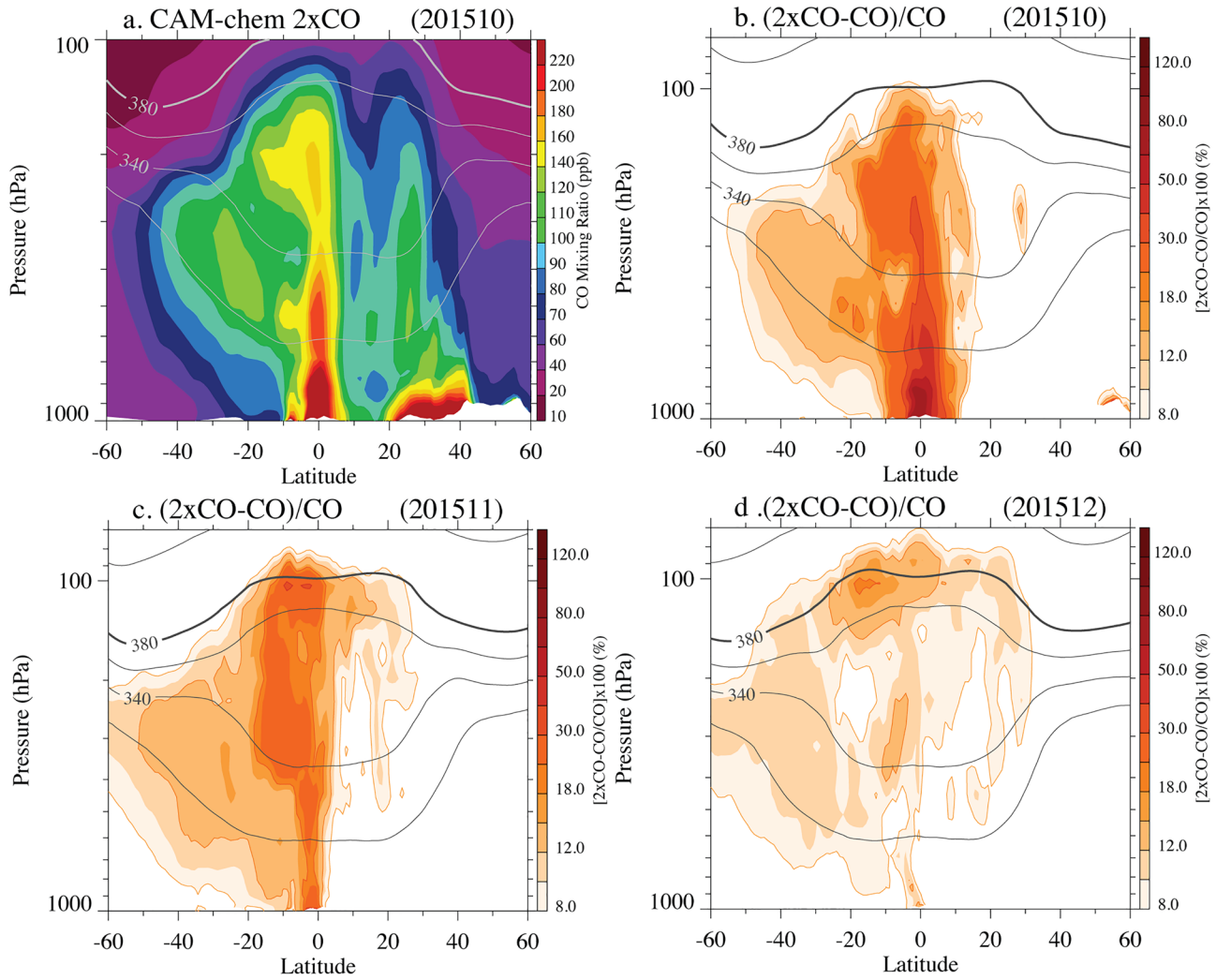

Figure 11. Latitude-altitude sections of (a) monthly mean CO (unit: ppbv) from CAM-chem 2 × CO simulation averaged between 110–120°E longitude and (b–d) differences in CO mixing ratios (unit:%) between CAM-chem 2 × CO and CO simulations [(2 × CO-CO)/CO × 100%] for (b) October, (c) November and (d) December 2015. Solid gray lines denote isentropes calculated from the CAM-chem simulations for the corresponding months. CAM-chem, Community Atmosphere Model with Chemistry.

A number of factors possibly contribute to the underestimated concentrations of CO in the CAM-chem simulations near the surface and also in the upper troposphere. As noted above, the difference between the surface CO from MOPITT and CAM-chem varies over different regions and ranges up to ~50% in Figure 8 over broad regions of EqAsia. We have clearly shown that CAM-chem CO is lower than the observations not only at the surface but also in the upper troposphere in October–December (Figures 8–10). This indicates that, as expected, underestimation of surface emissions has an impact on the amount of CO transported into the stratosphere. However, even with the lower surface emissions, the CO-EqAsia tracer from CAM-chem reproduces the transport pathway of CO emitted from wildfires into the tropical lower stratosphere in November–December 2015. To estimate the impact of increased surface emissions over Indonesia on tropical upper tropospheric CO, we performed a CAM-chem simulation with the amount of CO emitted from biomass burning being doubled over EqAsia relative to the emissions estimation in FINN. This sensitivity test is supported by the results of Nechita-Banda et al. (2018), who found that the amount of CO emissions in East Indonesia and Papua are double those reported by the FINN. This simulation is named "2 × CO" and the reference run is denoted "CO" in Figure 11. Figure 11a shows the monthly mean CO mixing ratios from the CAM-chem 2 × CO simulation over Indonesia (longitude: 110°–120°E) for October 2015. CO from the 2 × CO simulation has been increased compared to the reference run (Figure 7b) from the surface up to

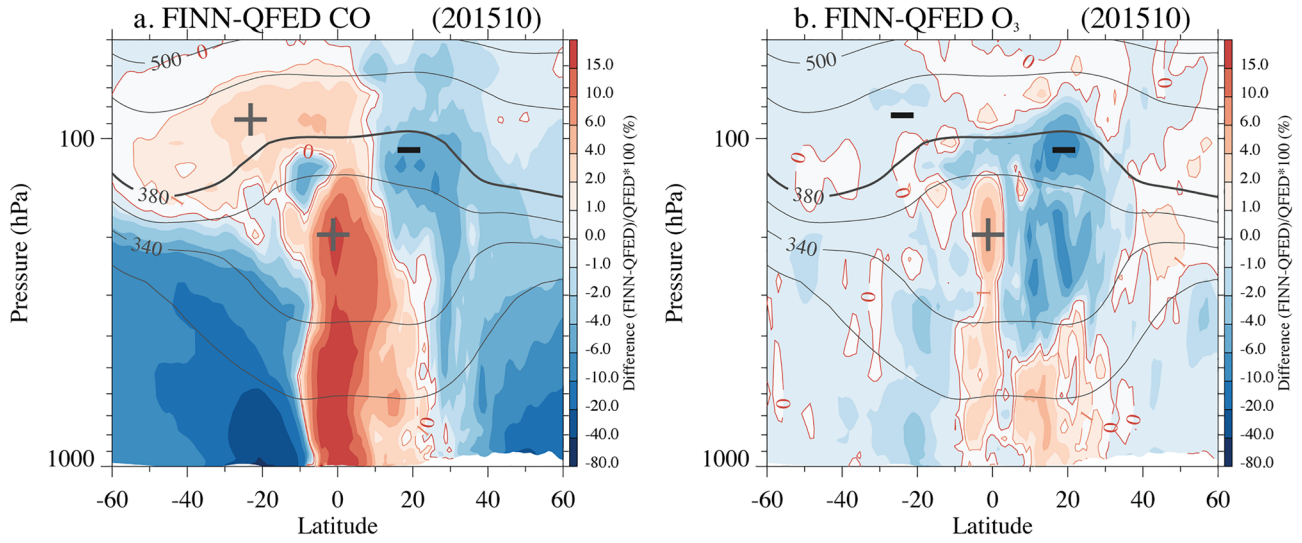

Figure 12. Latitude-altitude sections of differences in monthly mean (a) CO and (b) O_3 averaged between 100 and 120°E longitudes between CAM-chem simulations with FINN and QFED emissions for October 2015 (unit: %). CAM-chem, Community Atmosphere Model with Chemistry; FINN, Fire INventory from NCAR; QFED, Quick Fire Emissions Data Set.

~100 hPa in the tropical troposphere. CO in the subtropical mid-troposphere also shows an increase from ~90 to ~120 ppbv near 20°S and 30°N latitude. There is a maximum of up to ~150 ppbv in the tropical upper troposphere near ~200 hPa, which is considerably higher than the reference run but still lower than the MOPITT observations (Figures 7a and 7b).

The differences between the 2 × CO and CO simulations over Indonesia for each month from October to December 2015 are shown in Figures 11b–11d. The immediate response to the increased surface CO emission is obvious in October (Figure 11b). Positive CO anomalies not only prevail near the surface, but they also reach up to the mid-troposphere (~500 hPa), with a stronger signal at lower altitudes (~700 hPa). A secondary maximum in the CO differences appears in the tropical upper troposphere (~200 hPa), with a minimum in between those two altitudes. The increase in the upper tropospheric CO continues in November (Figure 11c) over wider latitude regions. Instead of showing a maximum in the tropics, the maxima in November are located off the equator, which indicates that not only vertical transport, but also horizontal transport contributes to the CO maxima. By December, the remnants of high CO have largely left the troposphere, but elevated CO remains evident in the uppermost troposphere and lower stratosphere (Figure 11d). The results of the 2 × CO simulation suggest that doubling CO emissions near the surface in October has an impact in the lower to upper troposphere, and ultimately has an impact on the transport of CO from the troposphere into the lower stratosphere after the fire season ends. This implies that if emissions from fire activity in Indonesia increase at the surface during the fire season, they will also perturb the upper troposphere and the stratosphere over the following months.

In addition to a shift in convection and transport due to the dynamical response to the El Niño itself, the implications of pollutants emitted from the wildfires associated with strong El Niño events include perturbations to tropospheric chemistry through direct emissions and photochemistry. Previous studies have shown that biomass burning increases CO and ozone in the TTL by changing both emissions and transport (e.g., Duncan, Bey, et al., 2003; Ducan, Strahan, et al., 2007; Ott et al., 2010). The OH concentration is decreased due to increased consumption by CO, heterogeneous chemistry and changes in UV light in the troposphere (see Duncan, Bey, et al., 2003 for details and references therein). Elevated CO in the troposphere also produces O_3 when NOx is present through NOx–HOx–CH_4–CO smog chemistry (Kinnison et al., 2001). In the lower stratosphere, the effects of elevated anthropogenic emissions on O_3 chemistry are more complex (Portmann et al., 2012). To assess the changes in O_3 in the tropical lower stratosphere (above the thermal tropopause) due to transport of CO from the Indonesian wildfires, we show in Figure 12 the differences in CO and O_3 between the two CAM-chem simulations run with FINN and QFED emissions for October 2015. We used exactly the same model configuration except the different CO emissions inventories to assess the

influence of lower CO emissions near the surface in the troposphere and lower stratosphere. Due to lower surface CO emissions in QFED, CAM-chem simulations with QFED emissions show lower mixing ratios of CO throughout the tropical troposphere. It is also clear in Figure 12a that differences in CO mixing ratios occur in the SH lower stratosphere up to ∼60 hPa. In the NH upper troposphere, the difference has the opposite sign (see the minus sign near 20°N). In Figure 12b, we show the differences in O_3 mixing ratios between the two model simulations. In the tropical upper troposphere, the CO and O_3 changes do have positive relationship, that is, more CO produces more O_3 (near 200 hPa in the tropics). In the SH lower stratosphere between the 380 and 500 K surfaces, there is negative change in ozone concentration where CO increases. The magnitude of the decrease in O_3 is relatively small and could be related to changes in both chemistry and transport. That is, enhanced vertical transport and convection can bring ozone poor air from the troposphere into the stratosphere. Increased CO and other pollutants can affect photolysis rates of ozone (Duncan, Bey, et al., 2003). This can have a long-lasting impact on O_3 chemistry and radiation in the stratosphere as CO from the fires can persist for long periods of time (see Figure 4). Further studies are needed to quantify the relative contributions of these effects.

7. Conclusions

In the tropical UTLS, temporal variations in CO are largely controlled by surface emissions, local convection and large-scale circulation (e.g., Jiang et al., 2007; Park et al., 2013; Randel et al., 2007; Schoeberl et al., 2006). Large-scale climate variability, such as El Niño, can have a significant influence on the surface emissions, convection and circulation, and hence on the temporal variability of CO in the tropical UTLS region. In this study, the global impact of anomalously high CO emitted during the 2015 El Niño event was characterized using both satellite measurements of CO in the troposphere and the stratosphere and a global chemistry transport model, CAM-chem. The MOPITT instrument has been providing vertical profiles of CO in the troposphere since 2000 (Deeter et al., 2019). Since 2004, Aura MLS has measured mixing ratios of CO with daily global coverage and relatively good vertical resolution in the upper troposphere and stratosphere. By combining the MOPITT and the MLS CO measurements, the spatial and temporal variability of CO is analyzed globally in the troposphere and the stratosphere.

Anomalously high mixing ratios of CO were observed by the MOPITT instrument in the lower to mid-troposphere during the active Indonesian fire season, September–October 2015, reaching the highest CO levels measured by the instrument since it began operations in 2000. The high CO was transported vertically and horizontally with up to ∼2 months of time lag in the upper troposphere. This is confirmed by the MLS CO measurements, which showed CO maxima at 147 and 100 hPa in November–December 2015 and later at higher altitudes (Figures 2–4). Anomalously high CO continued to be transported into the stratosphere and reached ∼40–50 hPa by the end of 2016. HCN measurements from the ACE-FTS and MLS instruments also showed significant impact from fires in Indonesia in the troposphere and the stratosphere (Pumphrey et al., 2018; Sheese et al., 2017). HCN, being almost exclusively produced by biomass burning, clearly showed the vertical transport of high HCN emitted from the wildfires into the tropical stratosphere, persisting throughout 2017 (Figure 5).

Simulations of CO from CAM-chem indicate a significant increase in CO mixing ratios in the tropical troposphere in October 2015. However, comparisons between CAM-chem and MOPITT CO suggest that the model underestimates the amount of CO in the tropical upper troposphere, as well as near the surface. However, tagged-CO simulations from CAM-chem are able to simulate the transport of CO emitted from wildfires into the stratosphere by December 2015. We performed a model simulation with doubled CO surface emissions from biomass burning over Indonesia for October 2015 (2 × CO simulation) to investigate the impact of higher surface emissions related to wildfires in CAM-chem. Comparisons with MOPITT CO suggest that the CAM-chem 2 × CO simulation still underestimates CO over Indonesia in October 2015. However, the 2 × CO simulation suggests that increasing emissions in October ultimately lead to increased model abundances of CO being transported into the lower stratosphere by December 2015. Further study should improve the CAM-chem simulations and deepen our understanding of the processes related to intense fire events. Three factors that can impact the model performance for this study the most include surface emissions, vertical transport, and chemistry included in the model. Among the chemical reactions included in the model, OH in particular plays an important role in controlling CO concentrations in the

troposphere. For instance, differences in OH concentrations can explain up to 50% in divergence in the magnitude of CO in various global models (Huijnen et al., 2019). It is also known that there is large uncertainty in the OH concentrations in the model (Huijnen et al., 2019; Zhao et al., 2019). Reducing the uncertainty in OH concentrations in the model can help to improve the model simulations and lead to better understanding of changes in chemical interactions.

We find that high concentrations of CO from the October 2015 Indonesian fires persisted not only in the troposphere but also in the tropical lower to mid stratosphere throughout 2016, much longer than in previous years with significant fire emissions. The model simulations suggest that more severe fire seasons in Indonesia will increase abundances of CO from fires in the stratosphere ~2–3 months later, with relatively small changes in ozone in the stratosphere. Persistent environmental changes in tropical peatland due to human activities will likely lead to increases in peatland fires and hence significant contributions to global carbon emissions (Page et al., 2002). Therefore, it is critical to understand the global impact of these fires and to be able to simulate transport of their emissions accurately with global chemistry models.

Data Availability Statement

The MOPITT CO gridded daily averages can be accessed at https://doi.org/10.5067/TERRA/MOPITT/MOP03J_L3.007. The MLS CO mixing ratio data are publicly available at https://doi.org/10.5067/Aura/MLS/DATA2005. The ACE-FTS data are available at http://www.ace.uwaterloo.ca and a registration is required. NCEP/NCAR Reanalysis data provided by the NOAA/OAR/ESRL PSD, Boulder, Colorado, USA, is downloaded from their web site at https://www.esrl.noaa.gov/psd/. Monthly mean zonal winds are downloaded from the website (http://www.geo.fu-berlin.de/en/met/ag/strat/produkte/qbo/index.html). The CAM-chem outputs used in this study are available at http://acomstaff.acom.ucar.edu/mijeong/camchem2015/

Acknowledgements
The authors thank the reviewers for their valuable comments. The National Center for Atmospheric Research is operated by the University Corporation for Atmospheric Research, under sponsorship of the National Science Foundation. The MOPITT team acknowledges the contributions of COMDEV and ABB BOMEM with support from the Canadian Space Agency (CSA), the Natural Sciences and Engineering Research Council (NSERC) and Environment Canada. The MOPITT and MLS projects are supported by the National Aeronautics and Space Administration (NASA) Earth Observing System (EOS) Program. The CESM project is supported primarily by the National Science Foundation (NSF). This material is based upon work supported by the National Center for Atmospheric Research, which is a major facility sponsored by the NSF under Cooperative Agreement No. 1852977. Computing and data storage resources, including the Cheyenne supercomputer (https://doi.org/10.5065/D6RX99HX), were provided by the Computational and Information Systems Laboratory (CISL) at NCAR. All simulations were carried out on the Cheyenne high-performance computing platform https://www2.cisl.ucar.edu/user-support/acknowledging-ncarcisl. Work at the Jet Propulsion Laboratory, California Institute of Technology, was done under contract with the National Aeronautics and Space Administration. Funding for the Atmospheric Chemistry Experiment comes primarily from the Canadian Space Agency.

References

Abalos, M., Legras, B., Ploeger, F., & Randel, W. J. (2015). Evaluating the advective Brewer-Dobson circulation in three reanalyses for the period 1979–2012. *Journal of Geophysical Research: Atmospheres*, *120*, 7534–7554. https://doi.org/10.1002/2015JD023182

Andreae, M. O. (2019). Emission of trace gases and aerosols from biomass burning - an updated assessment. *Atmospheric Chemistry and Physics*, *19*, 8523–8546. https://doi.org/10.5194/acp-19-8523-2019

Andreae, M. O., & Merlet, P. (2001). Emission of trace gases and aerosols from biomass burning. *Global Biogeochemical Cycles*, *15*, 955–966. https://doi.org/10.1029/2000GB001382

Baldwin, M. P., Gray, L. J., Dunkerton, T. J., Hamilton, K., Haynes, P. H., Randel, W. J., et al. (2001). The quasi-biennial oscillation. *Reviews of Geophysics*, *39*(2), 179–229. https://doi.org/10.1029/1999RG000073

Bernath, P. F. (2017). The Atmospheric Chemistry Experiment (ACE). *Journal of Quantitative Spectroscopy and Radiative Transfer*, *186*, 3–16. https://doi.org/10.1016/j.jqsrt.2016.04.006

Bernath, P. F., Boone, C. D., Walker, K. A., McLeod, S. D., & Nassar, R. (2005). Atmospheric Chemistry Experiment (ACE): Mission overview. *Geophysical Research Letters*, *32*, L15S01. https://doi.org/10.1029/2005GL022386

Bey, I., Jacob, D. J., Yantosca, R. M., Logan, J. A., Field, B. D., Fiore, A. M., et al. (2001). Global modeling of tropospheric chemistry with assimilated meteorology: Model description and evaluation. *Journal of Geophysical Research*, *106*(23), 23073–23095. https://doi.org/10.1029/2001JD000807

Boone, C. D., Bernath, P. F., Cok, D., Jones, S. C., & Steffen, J. (2020). Version 4 retrievals for the Atmospheric Chemistry Experiment Fourier Transform Spectrometer (ACE-FTS) and imagers. *Journal of Quantitative Spectroscopy and Radiative Transfer*, *247*, 106939. https://doi.org/10.1016/j.jqsrt.2020.106939

Boone, C. D., Nassar, R., Walker, K. A., Rochon, Y., McLeod, S. D., Rinsland, C. P., & Bernath, P. F. (2005). Retrievals for the Atmospheric Chemistry Experiment Fourier-transform spectrometer. *Applied Optics*, *44*, 7218–7231. https://doi.org/10.1364/AO.44.007218

Boone, C. D., Walker, K. A., & Bernath, P. F. (2013). Version 3 Retrievals for the Atmospheric Chemistry Experiment Fourier Transform Spectrometer (ACE-FTS). In P. Bernath (Ed.), *The Atmospheric Chemistry Experiment ACE at 10: A Solar Occultation Anthology* (pp. 103–127). A. Deepak Publishing.

Brasseur, G. P., & Solomon, S. (2005). Composition and chemistry. In *Aeronomy of the Middle Atmosphere* (Vol. 32). Atmospheric and Oceanographic Sciences Library. https://doi.org/10.1007/1-4020-3824-0_5

Butchart, N. (2014). The Brewer-Dobson circulation. *Reviews of Geophysics*, *52*, 157–184. https://doi.org/10.1002/2013RG000448

Chandra, S., Ziemke, J. R., Duncan, B. N., Diehl, T. L., Livesey, N. J., & Froidevaux, L. (2009). Effects of the 2006 El Niño on tropospheric ozone and carbon monoxide: Implications for dynamics and biomass burning. *Atmospheric Chemistry and Physics*, *9*, 4239–4249. https://doi.org/10.5194/acp-9-4239-2009

Clerbaux, C., George, M., Turquety, S., Walker, K. A., Barret, B., Bernath, P., et al. (2008). CO measurements from the ACE-FTS satellite instrument: Data analysis and validation using ground-based, airborne and spaceborne observations. *Atmospheric Chemistry and Physics*, *8*, 2569–2594. https://doi.org/10.5194/acp-8-2569-2008

Danabasoglu, G., Lamarque, J. F., Bacmeister, J., Bailey, D. A., DuVivier, A. K., Edwards, J., et al. (2020). The Community Earth System Model Version 2 (CESM2). *Journal of Advances in Modeling Earth Systems*, *12*, e2019MS001916. https://doi.org/10.1029/2019MS001916

Darmenov, A. S., & da Silva, A. M. (2015). *The Quick Fire Emissions Dataset (QFED)—Documentation of versions 2.1, 2.2 and 2.4. NASA/TM-2015-104606* (Vol. 38, p. 183). NASA Global Modeling and Assimilation Office. Retrieved from https://gmao.gsfc.nasa.gov/pubs/docs/Darmenov796.pdf

Deeter, M. N., Edwards, D. P., Francis, G. L., Gille, J. C., Mao, D., Martínez-Alonso, S., et al. (2019). Radiance-based retrieval bias mitigation for the MOPITT instrument: The version 8 product. *Atmospheric Measurement Techniques*, *12*, 4561–4580. https://doi.org/10.5194/amt-12-4561-2019

Deeter, M. N., Edwards, D. P., Francis, G. L., Gille, J. C., Martínez-Alonso, S., Worden, H. M., & Sweeney, C. (2017). A climate-scale satellite record for carbon monoxide: The MOPITT Version 7 product. *Atmospheric Measurement Techniques*, *10*, 2533–2555. https://doi.org/10.5194/amt-10-2533-2017

Deeter, M. N., Emmons, L. K., Edwards, D. P., Gille, J. C., & Drummond, J. R. (2004). Vertical resolution and information content of CO profiles retrieved by MOPITT. *Geophysical Research Letters*, *31*, L15112. https://doi.org/10.1029/2004GL020235

Deeter, M. N., Worden, H. M., Gille, J. C., Edwards, D. P., Mao, D., & Drummond, J. R. (2011). MOPITT multispectral CO retrievals: Origins and effects of geophysical radiance errors. *Journal of Geophysical Research*, *116*, D15303. https://doi.org/10.1029/2011JD015703

Diallo, M., Riese, M., Birner, T., Konopka, P., Müller, R., Hegglin, M. I., et al. (2018). Response of stratospheric water vapor and ozone to the unusual timing of El Niño and the QBO disruption in 2015-2016. *Atmospheric Chemistry and Physics*, *18*, 13055–13073. https://doi.org/10.5194/acp-18-13055-2018

Domeisen, D. I. V., Garfinkel, C. I., & Butler, A. H. (2019). The teleconnection of El Niño southern oscillation to the stratosphere. *Reviews of Geophysics*, *57*, 5–47. https://doi.org/10.1029/2018RG000596

Drummond, J. R., Zou, J., Nichitiu, F., Kar, J., Deschambaut, R., & Hackett, J. (2010). A review of 9-year performance and operation of the MOPITT instrument. *Advances in Space Research*, *45*, 760–774. https://doi.org/10.1016/j.asr.2009.11.019

Duncan, B. N., Bey, I., Chin, M., Mickley, L. J., Fairlie, T. D., Martin, R. V., & Matsueda, H. (2003). Indonesian wildfires of 1997: Impact on tropospheric chemistry. *Journal of Geophysical Research*, *108*(D15), 4458. https://doi.org/10.1029/2002jd003195

Duncan, B. N., Logan, J. A., Bey, I., Megretskaia, I. A., Yantosca, R. M., Novelli, P. C., et al. (2007). Global budget of CO, 1988-1997: Source estimates and validation with a global model. *Journal of Geophysical Research*, *112*(22), D22301. https://doi.org/10.1029/2007JD008459

Duncan, B. N., Martin, R. V., Staudt, A. C., Yevich, R., & Logan, J. A. (2003). Interannual and seasonal variability of biomass burning emissions constrained by satellite observations. *Journal of Geophysical Research*, *108*(D2), 4100. https://doi.org/10.1029/2002JD002378

Duncan, B. N., Strahan, S. E., Yoshida, Y., Steenrod, S. D., & Livesey, N. (2007). Model study of the cross-tropopause transport of biomass burning pollution. *Atmospheric Chemistry and Physics*, *7*, 3713–3736. https://doi.org/10.5194/acp-7-3713-2007

Edwards, D. P., Halvorson, C. M., & Gille, J. C. (1999). Radiative transfer modeling for the EOS Terra satellite Measurement of Pollution in the Troposphere (MOPITT) instrument. *Journal of Geophysical Research*, *104*(D14), 16755–16775. https://doi.org/10.1029/1999JD900167

Emmons, L. K., Schwantes, R. H., Orlando, J. J., Tyndall, G., Kinnison, D., Lamarque, J. F., et al. (2020). The chemistry mechanism in the Community Earth System Model version 2 (CESM2). *Journal of Advances in Modeling Earth Systems*, *12*, e2019MS001882. https://doi.org/10.1029/2019MS001882

Field, R. D., van der Werf, G. R., Fanin, T., Fetzer, E. J., Fuller, R., Jethva, H., et al. (2016). Indonesian fire activity and smoke pollution in 2015 show persistent nonlinear sensitivity to El Niño-induced drought. *Proceedings of the National Academy of Sciences of the United States of America*, *113*, 9204–9209. https://doi.org/10.1073/pnas.1524888113

Flury, T., Wu, D. L., & Read, W. G. (2013). Variability in the speed of the Brewer-Dobson circulation as observed by Aura/MLS. *Atmospheric Chemistry and Physics*, *13*, 4563–4575. https://doi.org/10.5194/acp-13-4563-2013

Folkins, I., Oltmans, S. J., & Thompson, A. M. (2000). Tropical convective outflow and near surface equivalent potential temperatures. *Geophysical Research Letters*, *27*(16), 2549–2552. https://doi.org/10.1029/2000GL011524

Gelaro, R., McCarty, W., Suárez, M. J., Todling, R., Molod, A., Takacs, L., et al. (2017). The modern-era retrospective analysis for research and applications, version 2 (MERRA-2). *Journal of Climate*, *30*(14), 5419–5454. https://doi.org/10.1175/JCLI-D-16-0758.1

Giglio, L., Csiszar, I., & Justice, C. O. (2006). Global distribution and seasonality of active fires as observed with the Terra and Aqua Moderate Resolution Imaging Spectroradiometer (MODIS) sensors. *Journal of Geophysical Research*, *111*, G02016. https://doi.org/10.1029/2005JG000142

Glatthor, N., Höpfner, M., Stiller, G. P., von Clarmann, T., Funke, B., Lossow, S., et al. (2015). Seasonal and interannual variations in HCN amounts in the upper troposphere and lower stratosphere observed by MIPAS. *Atmospheric Chemistry and Physics*, *15*, 563–582. https://doi.org/10.5194/acp-15-563-2015

Glatthor, N., von Clarmann, T., Stiller, G. P., Funke, B., Koukouli, M. E., Fischer, H., et al. (2009). Large-scale upper tropospheric pollution observed by MIPAS HCN and C2H6 global distributions. *Atmospheric Chemistry and Physics*, *9*(24), 9619–9634. https://doi.org/10.5194/acp-9-9619-2009

Guenther, A. B., Jiang, X., Heald, C. L., Sakulyanontvittaya, T., Duhl, T., Emmons, L. K., & Wang, X. (2012). The model of emissions of gases and aerosols from nature version 2.1 (MEGAN2.1): an extended and updated framework for modeling biogenic emissions. *Geoscientific Model Development*, *5*, 1471–1492. https://doi.org/10.5194/gmd-5-1471-2012

Harrison, M. E., Page, S. E., & Limin, S. H. (2009). The global impact of Indonesian forest fires. *Biologist*, *56*, 156–163.

Hoesly, R. M., Smith, S. J., Feng, L., Klimont, Z., Janssens-Maenhout, G., Pitkanen, T., et al. (2018). Historical (1750-2014) anthropogenic emissions of reactive gases and aerosols from the Community Emissions Data System (CEDS). *Geoscientific Model Development*, *11*, 369–408. https://doi.org/10.5194/gmd-11-369-2018

Holloway, T., Levy, H., & Kasibhatla, P. (2000). Global distribution of carbon monoxide. *Journal of Geophysical Research*, *105*, 12123–12147. https://doi.org/10.1029/1999jd901173

Holton, J. R., & Tan, H.-C. (1982). The Quasi-Biennial Oscillation in the Northern Hemisphere Lower Stratosphere. *Journal of the Meteorological Society of Japan*, *60*, 140–148. https://doi.org/10.2151/jmsj1965.60.1_140

Huang, L., Fu, R., & Jiang, J. H. (2014). Impacts of fire emissions and transport pathways on the interannual variation of CO in the tropical upper troposphere. *Atmospheric Chemistry and Physics*, *14*, 4087–4099. https://doi.org/10.5194/acp-14-4087-2014

Huang, L., Jiang, J. H., Murray, L. T., Damon, M. R., Su, H., & Livesey, N. J. (2016). Evaluation of UTLS carbon monoxide simulations in GMI and GEOS-Chem chemical transport models using Aura MLS observations. *Atmospheric Chemistry and Physics*, *16*, 5641–5663. https://doi.org/10.5194/acp-16-5641-2016

Huijnen, V., Pozzer, A., Arteta, J., Brasseur, G., Bouarar, I., Chabrillat, S., et al. (2019). Quantifying uncertainties due to chemistry modelling—Evaluation of tropospheric composition simulations in the CAMS model (cycle 43R1). *Geoscientific Model Development*, *12*, 1725–1752. https://doi.org/10.5194/gmd-12-1725-2019

Inness, A., Benedetti, A., Flemming, J., Huijnen, V., Kaiser, J. W., Parrington, M., & Remy, S. (2015). The ENSO signal in atmospheric composition fields: Emission-driven versus dynamically induced changes. *Atmospheric Chemistry and Physics*, *15*, 9083–9097. https://doi.org/10.5194/acp-15-9083-2015

Jiang, J. H., Livesey, N. J., Su, H., Neary, L., McConnell, J. C., & Richards, N. A. D. (2007). Connecting surface emissions, convective uplifting, and long-range transport of carbon monoxide in the upper troposphere: New observations from the Aura Microwave Limb Sounder. *Geophysical Research Letters*, *34*, L18812. https://doi.org/10.1029/2007GL030638

Khaykin, S., Legras, B., Bucci, S., Sellitto, P., Isaksen, L., Tencé, F., et al. (2020). The 2019/20 Australian wildfires generated a persistent smoke-charged vortex rising up to 35 km altitude. *Communications Earth & Environment*, *1*, 22. https://doi.org/10.1038/s43247-020-00022-5

Kiely, L., Spracklen, D. V., Wiedinmyer, C., Conibear, L., Reddington, C. L., Archer-Nicholls, S., et al. (2019). New estimate of particulate emissions from Indonesian peat fires in 2015. *Atmospheric Chemistry and Physics*, *19*, 11105–11121. https://doi.org/10.5194/acp-19-11105-2019

Kinnison, D. E., Connell, P. S., Rodriguez, J. M., Rotman, D. A., Considine, D. B., Tannahill, J., et al. (2001). The global modeling initiative assessment model: Application to high-speed civil transport perturbation. *Journal of Geophysical Research*, *106*(D2), 1693–1711. https://doi.org/10.1029/2000JD900406

Kistler, R., Collins, W., Saha, S., White, G., Woollen, J., Kalnay, E., et al. (2001). The NCEP-NCAR 50-year reanalysis: Monthly means CD-ROM and DOCUMENTATION. *Bulletin of the American Meteorological Society*, *82*, 247–267. https://doi.org/10.1175/1520-0477(2001)082<0247:TNNYRM>2.3.CO;2

Kleinböhl, A., Toon, G. C., Sen, B., Blavier, J. F. L., Weisenstein, D. K., Strekowski, R. S., et al. (2006). On the stratospheric chemistry of hydrogen cyanide. *Geophysical Research Letters*, *33*, L11806. https://doi.org/10.1029/2006GL026015

Lamarque, J.-F., Emmons, L. K., Hess, P. G., Kinnison, D. E., Tilmes, S., Vitt, F., et al. (2012). CAM-chem: Description and evaluation of interactive atmospheric chemistry in the Community Earth System Model. *Geoscientific Model Development*, *5*, 369–411. https://doi.org/10.5194/gmd-5-369-2012

Li, Q., Jacob, D. J., Bey, I., Yantosca, R. M., Zhao, Y., Kondo, Y., & Notholt, J. (2000). Atmospheric hydrogen cyanide (HCN): Biomass Burning source, ocean sink? *Geophysical Research Letters*, *27*, 357–360. https://doi.org/10.1029/1999GL010935

Liu, J., Logan, J. A., Murray, L. T., Pumphrey, H. C., Schwartz, M. J., & Megretskaia, I. A. (2013). Transport analysis and source attribution of seasonal and interannual variability of CO in the tropical upper troposphere and lower stratosphere. *Atmospheric Chemistry and Physics*, *13*, 129–146. https://doi.org/10.5194/acp-13-129-2013

Livesey, N. J., Read, W. G., Wagner, P. A., Froidevaux, L., Lambert, A., Manney, G. L., et al. (2020). *Version 4.2x Level 2 data quality and description document* (Technical. Report JPL D-33509 Rev. E). Jet Propulsion Lab. https://doi.org/10.1201/9780367816841

Logan, J. A., Megretskaia, I., Nassar, R., Murray, L. T., Zhang, L., Bowman, K. W., et al. (2008). Effects of the 2006 El Niño on tropospheric composition as revealed by data from the Tropospheric Emission Spectrometer (TES). *Geophysical Research Letters*, *35*, L03816. https://doi.org/10.1029/2007GL031698

Lohberger, S., Stängel, M., Atwood, E. C., & Siegert, F. (2018). Spatial evaluation of Indonesia's 2015 fire-affected area and estimated carbon emissions using Sentinel-1. *Global Change Biology*, *24*, 644–654. https://doi.org/10.1111/gcb.13841

Mahlman, J. D. (1997). Dynamics of Transport Processes in the Upper Troposphere. *Science*, *276*(5315), 1079–1083. https://doi.org/10.1126/science.276.5315.1079

Mead, M. I., Castruccio, S., Latif, M. T., Nadzir, M. S. M., Dominick, D., Thota, A., & Crippa, P. (2018). Impact of the 2015 wildfires on Malaysian air quality and exposure: A comparative study of observed and modeled data. *Environmental Research Letters*, *13*, 044023. https://doi.org/10.1088/1748-9326/aab325

Meinshausen, M., Vogel, E., Nauels, A., Lorbacher, K., Meinshausen, N., Etheridge, D. M., et al. (2017). Historical greenhouse gas concentrations for climate modelling (CMIP6). *Geoscientific Model Development*, *10*, 2057–2116. https://doi.org/10.5194/gmd-10-2057-2017

Minschwaner, K., Manney, G. L., Livesey, N. J., Pumphrey, H. C., Pickett, H. M., Froidevaux, L., et al. (2010). The photochemistry of carbon monoxide in the stratosphere and mesosphere evaluated from observations by the Microwave Limb Sounder on the Aura satellite. *Journal of Geophysical Research*, *115*, D13303. https://doi.org/10.1029/2009JD012654

Minschwaner, K., Su, H., & Jiang, J. H. (2016). The upward branch of the Brewer-Dobson circulation quantified by tropical stratospheric water vapor and carbon monoxide measurements from the Aura Microwave Limb Sounder. *Journal of Geophysical Research - D: Atmospheres*, *121*, 2790–2804. https://doi.org/10.1002/2015JD023961

Mote, P. W., Rosenlof, K. H., McIntyre, M. E., Carr, E. S., Gille, J. C., Holton, J. R., et al. (1996). An atmospheric tape recorder: The imprint of tropical tropopause temperatures on stratospheric water vapor. *Journal of Geophysical Research*, *101*, 3989–4006. https://doi.org/10.1029/95jd03422

Nassar, R., Logan, J. A., Megretskaia, I. A., Murray, L. T., Zhang, L., & Jones, D. B. A. (2009). Analysis of tropical tropospheric ozone, carbon monoxide, and water vapor during the 2006 El Niño using TES observations and the GEOS-Chem model. *Journal of Geophysical Research: Atmospheres*, *114*, D17304. https://doi.org/10.1029/2009jd011760

Naujokat, B. (1986). An update of the observed quasi-biennial oscillation of the stratospheric winds over the tropics. *Journal of the Atmospheric Sciences*, *43*, 1873–1877. https://doi.org/10.1175/1520-0469(1986)043<1873:auotoq>2.0.co;2

Nechita-Banda, N., Krol, M., van der Werf, G. R., Kaiser, J. W., Pandey, S., Huijnen, V., et al. (2018). Monitoring emissions from the 2015 Indonesian fires using CO satellite data. *Philosophical Transactions of the Royal Society B*, *373*, 20170307. https://doi.org/10.1098/rstb.2017.0307

Osman, M. K., Tarasick, D. W., Liu, J., Moeini, O., Thouret, V., Fioletov, V. E., et al. (2016). Carbon monoxide climatology derived from the trajectory mapping of global MOZAIC-IAGOS data. *Atmospheric Chemistry and Physics*, *16*, 10263–10282. https://doi.org/10.5194/acp-16-10263-2016

Osprey, S. M., Butchart, N., Knight, J. R., Scaife, A. A., Hamilton, K., Anstey, J. A., et al. (2016). An unexpected disruption of the atmospheric quasi-biennial oscillation. *Science*, *353*, 1424–1427. https://doi.org/10.1126/science.aah4156

Ott, L., Duncan, B., Pawson, S., Colarco, P., Chin, M., Randles, C., et al. (2010). Influence of the 2006 Indonesian biomass burning aerosols on tropical dynamics studied with the GEOS-5 AGCM. *Journal of Geophysical Research*, *115*, D14121. https://doi.org/10.1029/2009JD013181

Page, S. E., & Hooijer, A. (2016). In the line of fire: The peatlands of Southeast Asia. *Philosophical Transactions of the Royal Society B*, *371*, 20150176. https://doi.org/10.1098/rstb.2015.0176

Page, S. E., Siegert, F., Rieley, J. O., Boehm, H.-D. V., Jaya, A., & Limin, S. (2002). The amount of carbon released from peat and forest fires in Indonesia during 1997. *Nature*, *420*, 61–65. https://doi.org/10.1038/nature01131

Pan, X., Chin, M., Ichoku, C. M., & Field, R. D. (2018). Connecting Indonesian fires and drought with the type of El Niño and phase of the Indian Ocean Dipole during 1979–2016. *Journal of Geophysical Research: Atmospheres*, *123*, 7974–7988. https://doi.org/10.1029/2018JD028402

Park, M., Randel, W. J., Emmons, L. K., & Livesey, N. J. (2009). Transport pathways of carbon monoxide in the Asian summer monsoon diagnosed from Model of Ozone and Related Tracers (MOZART). *Journal of Geophysical Research*, *114*, D08303. https://doi.org/10.1029/2008JD010621

Park, M., Randel, W. J., Kinnison, D. E., Bourassa, A. E., Degenstein, D. A., Roth, C. Z., et al. (2017). Variability of stratospheric reactive nitrogen and ozone related to the QBO. *Journal of Geophysical Research - D: Atmospheres*, *122*, 103–110. https://doi.org/10.1002/2017JD027061

Park, M., Randel, W. J., Kinnison, D. E., Emmons, L. K., Bernath, P. F., Walker, K. A., et al. (2013). Hydrocarbons in the upper troposphere and lower stratosphere observed from ACE-FTS and comparisons with WACCM. *Journal of Geophysical Research: Atmospheres*, *118*, 1964–1980. https://doi.org/10.1029/2012JD018327

Pommrich, R., Müller, R., Grooß, J.-U., Günther, G., Konopka, P., Riese, M., et al. (2010). What causes the irregular cycle of the atmospheric tape recorder signal in HCN? *Geophysical Research Letters*, *37*, L16805. https://doi.org/10.1029/2010GL044056

Pommrich, R., Müller, R., Grooß, J.-U., Konopka, P., Ploeger, F., Vogel, B., et al. (2014). Tropical troposphere to stratosphere transport of carbon monoxide and long-lived trace species in the Chemical Lagrangian Model of the Stratosphere (CLaMS). *Geoscientific Model Development*, *7*, 2895–2916. https://doi.org/10.5194/gmd-7-2895-2014

Portmann, R. W., Daniel, J. S., & Ravishankara, A. R. (2012). Stratospheric ozone depletion due to nitrous oxide: Influences of other gases. *Philosophical Transactions of the Royal Society B*, *367*, 1256–1264. https://doi.org/10.1098/rstb.2011.0377

Pumphrey, H. C., Boone, C., Walker, K. A., Bernath, P., & Livesey, N. J. (2008). Tropical tape recorder observed in HCN. *Geophysical Research Letters*, *35*, L05801. https://doi.org/10.1029/2007GL032137

Pumphrey, H. C., Glatthor, N., Bernath, P. F., Boone, C. D., Hannigan, J. W., Ortega, I., et al. (2018). MLS measurements of stratospheric hydrogen cyanide during the 2015–2016 El Niño event. *Atmospheric Chemistry and Physics*, *18*, 691–703. https://doi.org/10.5194/acp-18-691-2018

Pumphrey, H. C., Santee, M. L., Livesey, N. J., Schwartz, M. J., & Read, W. G. (2011). Microwave Limb Sounder observations of biomass-burning products from the Australian bush fires of February 2009. *Atmospheric Chemistry and Physics*, *11*, 6285–6296. https://doi.org/10.5194/acp-11-6285-2011

Randel, W. J., & Cobb, J. B. (1994). Coherent variations of monthly mean total ozone and lower stratospheric temperature. *Journal of Geophysical Research*, *99*(D3), 5433–5447. https://doi.org/10.1029/93JD03454

Randel, W. J., Park, M., Emmons, L., Kinnison, D., Bernath, P., Walker, K. A., et al. (2010). Asian monsoon transport of pollution to the stratosphere. *Science*, *328*, 611–613. https://doi.org/10.1126/science.1182274

Randel, W. J., Park, M., Wu, F., & Livesey, N. (2007). A large annual cycle in Ozone above the tropical tropopause linked to the Brewer-Dobson circulation. *Journal of the Atmospheric Sciences*, *64*, 4479–4488. https://doi.org/10.1175/2007JAS2409.1

Rinsland, C. P., Salawitch, R. J., Osterman, G. B., Irion, F. W., Sen, B., Zander, R., et al. (2000). Stratospheric CO at tropical and mid-latitudes: ATMOS measurements and photochemical steady-state model calculations. *Geophysical Research Letters*, *27*(9), 1395–1398. https://doi.org/10.1029/1999GL011184

Santoso, A., Mcphaden, M. J., & Cai, W. (2017). The Defining characteristics of ENSO extremes and the strong 2015/2016 El Niño. *Reviews of Geophysics*, *55*, 1079–1129. https://doi.org/10.1002/2017RG000560

Sayer, A. M., Munchak, L. A., Hsu, N. C., Levy, R. C., Bettenhausen, C., & Jeong, M.-J. (2014). MODIS Collection 6 aerosol products: Comparison between Aqua's e-Deep Blue, Dark Target, and "merged" data sets, and usage recommendations. *Journal of Geophysical Research: Atmospheres*, *119*, 13965–13989. https://doi.org/10.1002/2014JD022453

Schoeberl, M. R., Douglass, A. R., Stolarski, R. S., Pawson, S., Strahan, S. E., & Read, W. (2008). Comparison of lower stratospheric tropical mean vertical velocities. *Journal of Geophysical Research*, *113*, D24109. https://doi.org/10.1029/2008JD010221

Schoeberl, M. R., Duncan, B. N., Douglass, A. R., Waters, J., Livesey, N., Read, W., & Filipiak, M. (2006). The carbon monoxide tape recorder. *Geophysical Research Letters*, *33*(12), L12811. https://doi.org/10.1029/2006GL026178

Schwartz, M. J., Santee, M. L., Pumphrey, H. C., Manney, G. L., Lambert, A., Livesey, N. J., et al. (2020). Australian new year's pyroCb impact on stratospheric composition. *Geophysical Research Letters*, *47*, e2020GL090831. https://doi.org/10.1029/2020GL090831

Sheese, P. E., Walker, K. A., & Boone, C. D. (2017). A global enhancement of hydrogen cyanide in the lower stratosphere throughout 2016. *Geophysical Research Letters*, *44*, 5791–5797. https://doi.org/10.1002/2017GL073519

Shi, Y. R., Levy, R. C., Eck, T. F., Fisher, B., Mattoo, S., Remer, L. A., et al. (2019). Characterizing the 2015 Indonesia fire event using modified MODIS aerosol retrievals. *Atmospheric Chemistry and Physics*, *19*, 259–274. https://doi.org/10.5194/acp-19-259-2019

Siegert, F., Zhukov, B., Oertel, D., Limin, S., Page, S. E., & Rieley, J. O. (2004). Peat fires detected by the BIRD satellite. *International Journal of Remote Sensing*, *25*, 3221–3230. https://doi.org/10.1080/01431160310001642377

Singh, H. B., Salas, L., Herlth, D., Kolyer, R., Czech, E., Viezee, W., et al. (2003). In situ measurements of HCN and CH3CN over the Pacific Ocean: Sources, sinks, and budgets. *Journal of Geophysical Research*, *108*(D20), 8795. https://doi.org/10.1029/2002JD003006

Sissenwine, N., Dubin, M., Teweles, S., & (COESA Co-Chairmen). (1976). *US Standard Atmosphere, Stock No. 003-017-00323-0*. US Government Printing Office.

Soukharev, B. E., & Hood, L. L. (2006). Solar cycle variation of stratospheric ozone: Multiple regression analysis of long-term satellite data sets and comparisons with models. *Journal of Geophysical Research*, *111*, D20314. https://doi.org/10.1029/2006JD007107

Stein, O., Schultz, M. G., Bouarar, I., Clark, H., Huijnen, V., Gaudel, A., et al. (2014). On the wintertime low bias of Northern Hemisphere carbon monoxide found in global model simulations. *Atmospheric Chemistry and Physics*, *14*, 9295–9316. https://doi.org/10.5194/acp-14-9295-2014

Tansey, K., Grégoire, J.-M., Defourny, P., Leigh, R., Pekel, J.-F., van Bogaert, E., & Bartholomé, E. (2008). A new, global, multi-annual (2000–2007) burnt area product at 1 km resolution. *Geophysical Research Letters*, *35*, L01401. https://doi.org/10.1029/2007GL031567

Tilmes, S., Hodzic, A., Emmons, L. K., Mills, M. J., Gettelman, A., Kinnison, D. E., et al. (2019). Climate forcing and trends of organic aerosols in the Community Earth System Model (CESM2). *Journal of Advances in Modeling Earth Systems*, *11*, 4323–4351. https://doi.org/10.1029/2019MS001827

Tolton, B. T., & Drummond, J. R. (1997). Characterization of the length-modulated radiometer. *Applied Optics*, *36*, 5409–5420. https://doi.org/10.1364/AO.36.005409

Tweedy, O. V., Kramarova, N. A., Strahan, S. E., Newman, P. A., Coy, L., Randel, W. J., et al. (2017). Response of trace gases to the disrupted 2015–2016 quasi-biennial oscillation. *Atmospheric Chemistry and Physics*, *17*, 6813–6823. https://doi.org/10.5194/acp-17-6813-2017

van der Werf, G. R., Randerson, J. T., Giglio, L., Collatz, G. J., Kasibhatla, P. S., & Arellano, A. F., Jr (2006). Interannual variability in global biomass burning emissions from 1997 to 2004. *Atmospheric Chemistry and Physics*, *6*, 3423–3441. https://doi.org/10.5194/acp-6-3423-2006

van der Werf, G. R., Randerson, J. T., Giglio, L., Collatz, G. J., Mu, M., Kasibhatla, P. S., et al. (2010). Global fire emissions and the contribution of deforestation, savanna, forest, agricultural, and peat fires (1997–2009). *Atmospheric Chemistry and Physics*, *10*, 11707–11735. https://doi.org/10.5194/acp-10-11707-2010

van der Werf, G. R., Randerson, J. T., Giglio, L., van Leeuwen, T. T., Chen, Y., Rogers, B. M., et al. (2017). Global fire emissions estimates during 1997–2016. *Earth System Science Data*, *9*, 697–720. https://doi.org/10.5194/essd-9-697-2017

Wallace, J. M. (1973). General circulation of the tropical lower stratosphere. *Reviews of Geophysics*, *11*(2), 191–222. https://doi.org/10.1029/RG011i002p00191

Wallace, J. M., Panetta, R. L., & Estberg, J. (1993). Representation of the equatorial stratospheric quasi-biennial oscillation in EOF phase space. *Journal of the Atmospheric Sciences*, *50*, 1751–1762. https://doi.org/10.1175/1520-0469(1993)050<1751:rotesq>2.0.co;2

Waters, J. W., Froidevaux, L., Harwood, R. S., Jarnot, R. F., Pickett, H. M., Read, W. G., et al. (2006). The Earth Observing System Microwave Limb Sounder (EOS MLS) on the Aura satellite. *IEEE Transactions on Geoscience and Remote Sensing*, *44*(5), 1075–1092. https://doi.org/10.1109/TGRS.2006.873771

Wiedinmyer, C., Akagi, S. K., Yokelson, R. J., Emmons, L. K., Al-Saadi, J. A., Orlando, J. J., & Soja, A. J. (2011). The Fire INventory from NCAR (FINN): A high resolution global model to estimate the emissions from open burning. *Geoscientific Model Development*, *4*, 625–641. https://doi.org/10.5194/gmd-4-625-2011

Wolter, K., & Timlin, M. S. (1993). Monitoring ENSO in COADS with a seasonally adjusted principal component index. In *Proceedings of the 17th Climate Diagnostics Workshop* (pp. 52–57). NOAA/NMC/CAC, NSSL, Oklahoma Clim. Survey, CIMMS and the School of Meteor, University of Oklahoma. Retrieved from http://www.cdc.noaa.gov/people/klaus.wolter/MEI

Worden, H. M., Deeter, M. N., Edwards, D. P., Gille, J. C., Drummond, J. R., & Nédélec, P. (2010). Observations of near-surface carbon monoxide from space using MOPITT multispectral retrievals. *Journal of Geophysical Research*, *115*, D18314. https://doi.org/10.1029/2010JD014242

Worden, H. M., Deeter, M. N., Frankenberg, C., George, M., Nichitiu, F., Worden, J., et al. (2013). Decadal record of satellite carbon monoxide observations. *Atmospheric Chemistry and Physics*, *13*, 837–850. https://doi.org/10.5194/acp-13-837-2013

Zhao, Y., Saunois, M., Bousquet, P., Lin, X., Berchet, A., Hegglin, M. I., et al. (2019). Inter-model comparison of global hydroxyl radical (OH) distributions and their impact on atmospheric methane over the 2000–2016 period. *Atmospheric Chemistry and Physics*, *19*, 13701–13723. https://doi.org/10.5194/acp-19-13701-2019

Ziemke, J. R., Chandra, S., McPeters, R. D., & Newman, P. A. (1997). Dynamical proxies of column ozone with applications to global trend models. *Journal of Geophysical Research*, *102*, 6117–6129. https://doi.org/10.1029/96JD03783